Pauli blocking in the low-lying, low-spin states of ^{141}Pr

M. Scheck,[1,*] S. N. Choudry,[1] E. Elhami,[1] M. T. McEllistrem,[1] S. Mukhopadhyay,[1] J. N. Orce,[1] and S. W. Yates[1,2]
[1]*Dept. of Physics & Astronomy, University of Kentucky, Lexington, Kentucky 40506-0055, USA*
[2]*Dept. of Chemistry, University of Kentucky, Lexington, Kentucky 40506-0055, USA*
(Received 23 June 2008; published 2 September 2008; publisher error corrected 17 September 2008)

The low-lying, low-spin levels of ^{141}Pr were investigated using $(n, n'\gamma)$ techniques. Level energies, branching ratios, and tentative spin assignments for more than 100 states, linked by nearly 300 transitions, were obtained from two angular distributions ($E_n = 2.0$ and 3.0 MeV) and an excitation function measurement ($E_n = 1.5$–3.2 MeV). The application of the Doppler-shift attenuation method led to the determination of lifetimes. The obtained spectroscopic data provide insight into the wave functions of the states observed. A detailed analysis of the $[2_1^+ \otimes d_{5/2}]$ and $[2_1^+ \otimes g_{7/2}]$ multiplets provides the first quantitative evidence for Pauli blocking in a spherical odd-mass nucleus. The unpaired particle is used to probe the microscopic structure of the first 2^+ state of the adjacent core nuclei ^{140}Ce and ^{142}Nd.

DOI: 10.1103/PhysRevC.78.034302 PACS number(s): 21.10.Re, 21.30.Fe, 25.40.Fq, 27.60.+j

I. INTRODUCTION AND MOTIVATION

While the understanding of low-lying, low-spin collective excitations in even-even mass nuclei near or at closed shells has improved in recent years, the behavior of particle-core coupled states in odd-mass nuclei remains a challenge. Below the pairing gap, spherical even-even nuclei show only a limited number of excitations, e.g., isoscalar quadrupole and octupole phonon excitations and their various couplings, and mixed-symmetry isovector quadrupole excitations [1–4]. Even when the observed level density is moderate, state-mixing and blocking effects in higher phonon orders due to the microscopic structure of the phonons cause deviations from the vibrational decay patterns expected in a naive, macroscopic picture. In odd-mass nuclei, collective states of particle-core coupling nature [5,6] are expected alongside single-particle states, and the increased level density results in a much larger mixing of the close-lying excitations. Of particular interest for odd-mass nuclei is the question of how the even-mass collective core excitations, which must be built up by pairs of nucleons coupled to integer spins forming a bosonic degree of freedom, are disturbed in the presence of the additional fermion. Theoretical approaches within the BCS [7] predict a lowering of the pairing energy. Furthermore, in such systems as the nucleus with a configuration space consisting of a finite number of m substates, a lowering in the average quasiparticle boson number is expected. In the particle picture, this corresponds to a truncation of the valence space due to Pauli blocking.

In a macroscopic approach neglecting the underlying structure of the core excitation, spherical odd-mass nuclei are usually described by coupling the unpaired particle to the states of the neighboring even-even core nuclei. In the limit of weak coupling of the unpaired particle or hole to the neighboring even-even core nucleus, the particle orbits in the slightly deformed field generated by the dynamical deformation of the core excitation. The single core excitation $J_C^{\pi_C}$ splits into a multiplet $[J_C^{\pi_C} \otimes J_p^{\pi_p}]_J^{\pi_C \pi_p}$. Here, J_C and J_p are the angular momenta and π_C and π_p are the parities of the core and the unpaired particle, respectively. The coupled states are expected to decay with the same multipole character as the core excitation, and the transition strength will be fragmented into several weaker transitions from the states of the multiplet. Nevertheless, in the weak-coupling limit, the sum of the excitation strength is expected to be conserved [8]:

$$B(\Pi L) \uparrow = \sum_J B(\Pi L) \uparrow_J . \tag{1}$$

The strength-weighted averaged excitation energy of the resulting multiplet, often referred to as the center of gravity, is defined as

$$\langle E \rangle = \frac{\sum_J E_J B(\Pi L) \uparrow_J}{\sum_J B(\Pi L) \uparrow_J} \tag{2}$$

and is, within this simple model, expected to be the same as the energy of the collective core excitation. For low-lying particle-core coupled multiplets, the center of gravity is usually shifted slightly to lower energies in comparison to the core excitation because of mixing with higher lying states. For example, calculations in the quasiparticle phonon model (QPM) [9,10] for $[[2_1^+ \otimes 3_1^-] \otimes particle]$, coupled states in ^{115}In [11] and ^{117}Sn [12,13] reproduce the experimentally observed energies and degree of fragmentation only when phonon couplings of the third order are considered.

Usually, odd-mass nuclei also exhibit low-lying excited states corresponding to an excitation of the unpaired particle into another subshell, which gives rise to further $[J_C^{\pi_C} \otimes J_p^{\pi_p}]_{J^\pi}$ multiplets. In cases where the energy gap between the ground state and an excited single-particle state is small, their multiplets are within the same energy region. As the identical core components of the wave functions have a large overlap, states with the same spin and parity from the different multiplets are expected to mix heavily. Furthermore, mixing with other excitations of higher or lower phonon order and single-particle states have to be considered.

*Present address: Oliver Lodge Laboratory, Dept. of Physics, University of Liverpool, Liverpool L69 7ZE, U.K.

Because of the heavy mixing, the wave functions of the states in odd-mass nuclei consist of multiple components with different origins. Within the particle-core coupling picture, a realistic wave function of a low-lying state with the total angular momentum J for an odd-mass nucleus can be written as

$$|\Psi\rangle_J = \alpha|p_i\rangle_J + \sum_j \sum_m \beta_{jm}|Q_j^+ \otimes p_m\rangle_J + \sum_{kl} \sum_i \sum_n \gamma_{(kl)_i n}|[Q_k^+ \otimes Q_l^+]_{J_i} \otimes p_n\rangle_J + \text{h.o.} \quad (3)$$

Here, $\alpha, \beta_{jm}, \gamma_{(kl)_i n}$ are the mixing amplitudes, $Q_{j,k,l}^+$ stands for the various excitations in the even-even core nucleus, $[Q_k^+ \otimes Q_l^+]_{J_i}$ represents phonon couplings of second order coupled to the respective angular momentum J_i, and $p_{i,j,m}$ denotes the unpaired particle in a subsequent subshell. The first term describes a single-particle excitation from one subshell to another. The second term describes the coupling of a particle to a one-phonon excitation. At minimum, this is the interaction of the unpaired particle in the ground state, but it can also describe the couplings of low-energy single-particle excitations forming additional particle-core coupled multiplets, thus one has to consider the mixing among these structures. The summation over different Q_j^+ takes either the isoscalar or isovector states of the same phonon order into account or, within the boson mapping of the QPM, phonons of the same angular momentum but different microscopic structures, distinguished within the QPM by the root quantum number i. In the QPM, the lowest-lying RPA phonon Q_1^+ of a given spin usually has the most collective structure. The collectivity decreases with increasing root quantum number, thus the higher lying phonons end up as nearly pure two-quasiparticle excitations. The third term describes the admixture of structures with the respective particle coupled to a phonon coupling of second order.

While the single-particle component in the wave functions can be measured directly using particle-transfer reactions [e.g., $(d,{}^3\text{He})$], the other amplitudes in Eq. (3) are best investigated by measuring the decay behavior such as the reduced transition probabilities and the multipole character of the transitions connecting different states.

A semimagic nucleus like the $N = 82$ isotone ^{141}Pr has the advantage that some constituents in Eq. (3) do not occur. The $N = 82$ shell closure, in which no low-lying particle-hole-like intruder states [14] are found, keeps the neutrons almost inert, thus isovector excitations are excluded. The underlying proton shell structure has been investigated using ^{140}Ce(d, n) [15], ^{140}Ce(^{3}He,d) [16], and ^{140}Ce(^{7}Li, ^{6}He) [17] single-nucleon transfer reactions. The results of these experiments indicate a subshell closure between the ground state consisting of the proton in the $2d_{5/2}$ subshell, the first excited state ($E =$ 145 keV) corresponding to a proton hole in the $1g_{7/2}$ subshell, and the group with the $1h_{11/2}(E = 1117$ keV), $2d_{3/2}(E =$ 1608 keV), and the fragmented $3s_{1/2}(E = 1299$ and $E =$ 1651 keV) subshells. As a consequence, below 2.5 MeV ($\approx E_{2^+_{\text{core}}} + E_{3s_{1/2}}$), the subshell closure reduces the number of particles p_i that have to be considered in Eq. (3) to the proton in the $2d_{5/2}$ subshell and the hole in the $1g_{7/2}$ subshell.

A direct consequence of this limited valence space is the high excitation energies of the lowest collective states in the semimagic core nuclei ^{140}Ce ($E_{2^+} = 1596$; $E_{3^-} = 2464$ keV) and ^{142}Nd ($E_{2^+} = 1576$; $E_{3^-} = 2084$ keV) [18]. The level sequence of both core nuclei points toward most observed excitations having a nearly pure two-particle structure. The fact that the first excited 4^+ and 6^+ levels lie close to each other and just above the pairing gap indicates a $[g_{7/2}]^2$ origin. QPM calculations for ^{140}Ce [19] have shown the major components (50%) of the wave function of the first 2^+ state to be $[g_{7/2}]^2$. Admixtures of $[d_{5/2}]^2(21\%)$, $[g_{7/2}, d_{5/2}](7\%)$, and other configurations such as $[h_{11/2}]^2$ cause the energy of this state to be lowered. For ^{142}Nd, the weighting of the different components of the first 2^+ excitation is expected to be shifted smoothly from the $[g_{7/2}]^2$ to the $[d_{5/2}]^2$ component [20]. The decrease of the excitation energy of the 3^- octupole phonon with increasing proton number, caused by the reduction of the subshell gap due to a smaller energy difference between the $d_{5/2}$ and $h_{11/2}$ subshells (see Fig. 7.17 in Ref. [21]), as well as by an increase of the Fermi level (Fig. 7.10 in Ref. [21]), indicates a more important role of the $[h_{11/2}]^2$ component in the wave functions of the quadrupole phonons. The state sequence expected for the $[g_{7/2}, d_{5/2}]$ two-particle configuration ($J^\pi = 1^+$ to 6^+) is found in both core nuclei at approximately 2.5 MeV. The second 0^+ state in ^{140}Ce at 1903 keV is known to decay to the first 2^+ state with a similar transition strength as observed for the $2_1^+ \rightarrow 0_1^+$ transition. However, the strongly deviating excitation energy makes the assignment as a two-phonon candidate unlikely. In general, it can be stated that the gap between the two subshell groups and the resulting limited collectivity leads to extreme deviations from the naive macroscopic phonon picture, thus both core nuclei can be seen as exhibiting an onset of collectivity, as observed for their first 2^+ quadrupole excitations. Astonishingly, the phonon picture seems to apply for the quadrupole-octupole two-phonon excitations. In (γ, γ') experiments, the $[2^+ \otimes 3^-]_{1^-}$ states were found near the sum energy of the coupling phonons [22–24], deviating with only small anharmonicities (see Fig. 1).

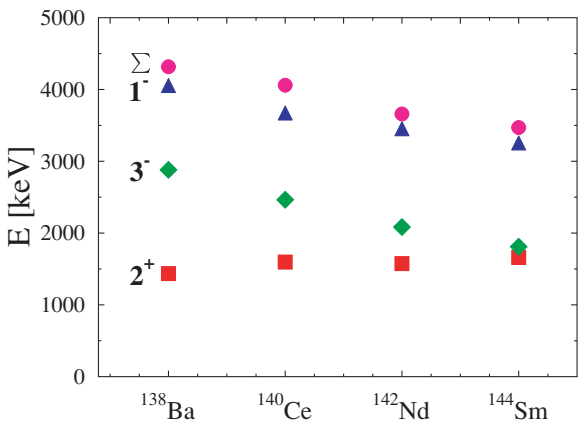

FIG. 1. (Color online) Excitation energies of the first 2^+ (red square), 3^- (green diamond) states, and the $[2^+ \otimes 3^-]_{1^-}$ states (blue triangle) compared with the sum energy (magenta circle) of the 2^+ and 3^- excitations for some even-even $N = 82$ isotones.

This study of ^{141}Pr was motivated by a recent inelastic photon scattering experiment [25] in which only 60% of the $E1$ strength for the quadrupole-octupole-particle coupled states $[[2^+ \otimes 3^-] \otimes p]$ was observed compared to that for the $[2^+ \otimes 3^-]_{1^-}$ two-phonon states in the adjacent core nuclei. However, in the photon scattering experiments, it could not be completely excluded that some $E1$ strength was lost to unobserved transitions feeding lower lying excited states and, therefore, was simply hidden in the huge nonresonant background. If the reduced strength is indeed a nuclear structure effect, the multiplicative nature of the $E1$ operator $[B(E1) \uparrow \propto \beta_2\beta_3]$ [26,27] predicts a paucity of strength in the phonon-particle coupled multiplets of the two constituent phonons. Therefore, using an experimental technique in which all the $2^+ \otimes p_i$ and $3^- \otimes p_i$ coupled states are populated in combination with a method for lifetime measurements offers the opportunity to test whether the lack of $E1$ strength for the quadrupole-octupole-particle coupled states was just an experimental problem or if, as suggested in Ref. [25], it is the consequence of Pauli blocking due to the presence of the unpaired proton in the subshells required for the microscopic structure of the participating one-phonon states.

In the following, a brief overview of the experimental techniques is given in Sec. II, the data are presented in Sec. III, and the results are discussed in Sec. IV.

II. EXPERIMENTS

For the investigation of the low-lying, low-spin level scheme of a stable nucleus, inelastic neutron scattering (INS) [28] has the advantage that all levels, independent of their microscopic nature, are statistically populated. Together with the high resolution of modern high-purity germanium (HPGe) detectors, this population enables the observation of the detailed decay scheme up to the energy of the incident neutrons. The only restriction on the excitation of a state within the excitation energy range is the maximum angular momentum transfer by the incident neutron, typically $\Delta J \leqslant 6$, with respect to the ground state spin J_0. In combination with the Doppler-shift attenuation method (DSAM) for lifetime measurements, INS is a powerful tool for nuclear structure studies.

The INS experiments were performed at the neutron scattering facility at the 7 MV Van de Graaff accelerator of the University of Kentucky. A pulsed and bunched proton beam ($\nu = 1.875$ MHz, $\Delta t \approx 2$ ns) incident on a tritium-filled gas cell produced monoenergetic neutrons ($\Delta E_n \approx 60$ keV at $E_n = 2$ MeV) via the ^{3}H$(p, n)^3$He reaction. The scattering sample was located at a distance of 6 cm from the end of the tritium gas cell and consisted of 49.28 g of $^{141}Pr_2O_3$ in a cylindrical geometry ($h = 4$ cm, $\text{ø} = 2$ cm). The γ rays emitted from the excited target nuclei were detected with a HPGe detector (full width at half maximum at 1.3 MeV $\approx$1.8 keV, with a relative efficiency of 55%) at 118 cm from the scattering sample. The detector was shielded with an active anti-Compton bismuth germanate (BGO) suppression shield along with passive shielding of tungsten, lead, copper, and polyethylene. A time-of-flight gate on the incoming bunched proton beam was applied for further background reduction. A typical γ-ray spectrum recorded during the excitation function

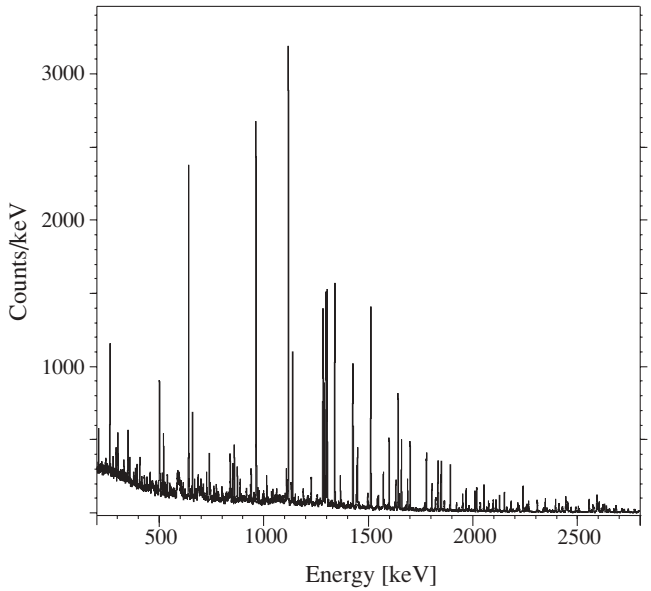

FIG. 2. Typical γ-ray spectrum ($E_n = 3.2$ MeV) recorded for the excitation function measurements of ^{141}Pr. The large number of observed γ rays and the high quality of the data are obvious.

measurements is shown in Fig. 2. Even in this full-scale plot, the high quality of the spectra and the large number of resolved γ rays are obvious. The energy and detector efficiency calibrations were performed using a ^{226}Ra source in a separate off-line calibration.

Three different measurements were conducted: an excitation function measurement from $E_n = 1.5$ to 3.2 MeV in steps of 75 keV and angular distribution measurements at $E_n = 2.0$ and 3.0 MeV. Typical examples of γ-ray excitation functions [Yield$(E_n) = \sum_i Y_{\gamma_i}(E_n)$; $\Delta Y = \sqrt{\sum_i Y_i^2}$] are shown in Fig. 3. The onset corresponds to the level energy from which the γ ray is emitted, and a deviation in the yield indicates a

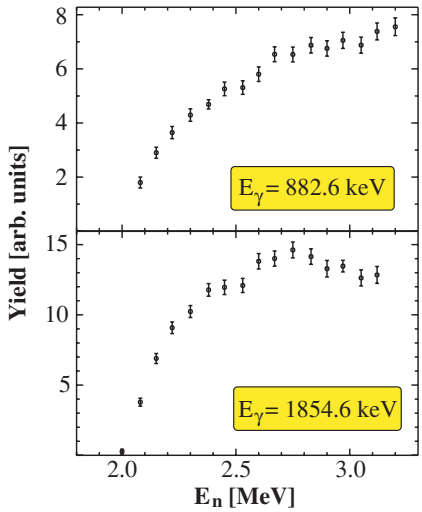

FIG. 3. (Color online) Examples of γ-ray excitation functions. These transitions were previously assigned to arise from a single level at 2000 keV. The obvious discrepancies in the yields with increasing energy led to the assignment of states at 1999.8 and 2000.4 keV.

feeding level at the respective energy. Previously, both γ rays in Fig. 3 were assigned as decaying from the same level [18], but the different shapes lead to the conclusion that they originate from different states at nearly identical energies. The shape contains information about the angular momentum transfer in the neutron scattering process and the density of states of a given spin which compete for the partial waves of the incident neutron. Therefore, the comparison of the experimentally observed level excitation function with theoretical predictions calculated with the statistical model computer code CINDY [29] contains information about the spin of the excited level. As any missing transitions will reduce the total observed yield, a detailed knowledge of the level scheme is necessary. For normalization of the spectra at different neutron energies, the total number of neutrons for each energy was recorded using a BF_3-filled proportional counter with a geometry designed to provide a flat response to neutrons. Additionally, the experimentally observed yield curve must be corrected for the photon absorption [30] and neutron attenuation in the scattering sample itself. Furthermore, the dependence of the inelastic neutron cross sections [31] at the initial neutron energy has to be considered. After all corrections to the data were made, the experimental values were normalized to the calculated cross sections.

Angular distributions were recorded at nine angles between 40° and 150° with respect to the primary beam. Several spins were assigned, and for a number of transitions multipole-mixing ratios δ were obtained. Unfortunately, for INS experiments on odd-mass nuclei, if the spin of an excited state equals or is smaller than the ground-state spin, the angular distribution is isotropic [32], and neither a spin assignment nor the determination of a multipole-mixing ratio is possible. The anisotropy of an angular distribution also is perturbed, or even destroyed, if the state is fed excessively from higher lying levels.

The Doppler-shift attenuation method (DSAM) was applied to the spectra recorded in the angular distribution measurements. The Doppler-shifted peak energy is dependent on the scattering angle and is given by

$$E_\gamma(\Theta) = E_\gamma(90^\circ)[1 + \beta F(\tau)\cos\Theta]. \quad (4)$$

The reaction kinematics of the inelastic neutron scattering reaction are included in the factor

$$\beta = \frac{v_{\text{c.m.}}}{c} = 0.04635\frac{A_n}{A_n + A_{^{141}Pr}}\sqrt{\frac{E_n}{A_n}}. \quad (5)$$

Obviously, the initial neutron energy E_n and the masses A_i determine β. The attenuation factor $F(\tau)$ takes the interaction of the recoiling nucleus and the surrounding medium into account. For the analysis, $F(\tau)$ was calculated using the Winterborn formalism [33], which relates the stopping power of the material in which the excited nucleus recoils to the lifetime of the excited state. Examples are shown in Fig. 4. Typically, lifetimes in the femtosecond range are accessible using the DSAM. As with the angular distribution measurements, feeding affects the lifetime determination. With the emission of the first γ ray, the recoiling nucleus decelerates, thus the kinematics of the nucleus has changed for the emission of the second γ ray. The γ ray appears less shifted and, consequently, the lifetime appears to be longer. To minimize these feeding effects, angular distribution measurements were conducted at two different energies ($E_n = 2.0$ and $E_n = 3.0$ MeV). A ^{24}Na radioactive source and the 2223 keV proton-neutron capture line were used for an online calibration of the γ-ray spectra and to monitor and correct for electronic shifts.

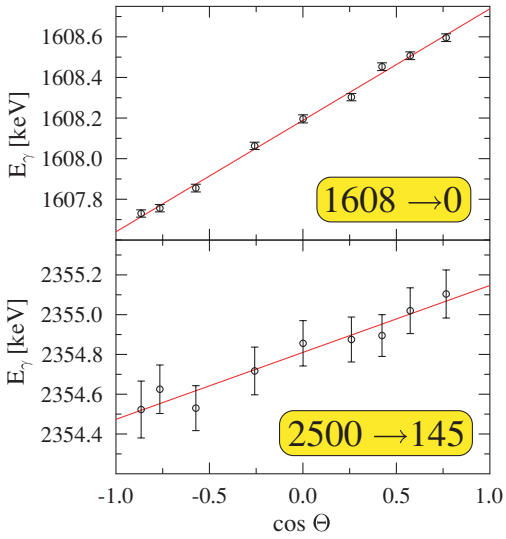

FIG. 4. (Color online) Example plots of $E_\gamma(\Theta)$ vs $\cos\Theta$. The gradient of the straight lines contains the information about the attenuation factor $F(\tau)$.

III. EXPERIMENTAL DATA

In total, over 300 γ rays were observed. Using the information obtained in the excitation function measurement (threshold and shape) and the observed lifetimes, it was possible to place about 280 γ rays in a level scheme consisting of 101 levels. The observed levels are shown in comparison with the level sequences of the core nuclei ^{140}Ce and ^{142}Nd in Fig. 5. The γ rays that could not be placed in the level scheme are given in Table I, together with the lowest neutron energies at which each γ ray was observed in the excitation function measurements.

For the spin assignments, the level excitation functions and the angular distribution data were reviewed, and the decay behavior was taken into account. To exclude the effects

TABLE I. Observed γ rays that could not be placed in the level scheme. Given are the γ-ray energy E_γ and the lowest neutron energy E_n at which the γ ray was observed.

E_γ (keV)	E_n (MeV)	E_γ (keV)	E_n (MeV)
261.46(18)	2.05	1019.31(30)	2.60
270.06(22)	2.52	1129.32(32)	2.52
461.95(18)	2.37	1153.24(37)	2.75
582.31(27)	2.90	1233.06(34)	2.90
709.09(27)	2.60	1384.51(35)	2.75
711.96(20)	2.52	1467.87(41)	2.75
787.75(31)	2.90	1481.28(36)	2.67
918.06(39)	2.90		

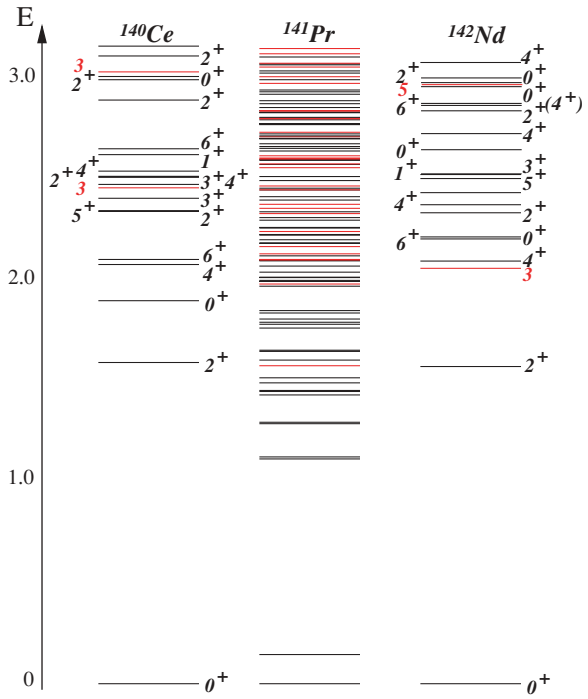

FIG. 5. (Color online) Levels of ^{141}Pr compared with those in the core nuclei ^{140}Ce and ^{142}Nd. States with a probable negative parity are in red.

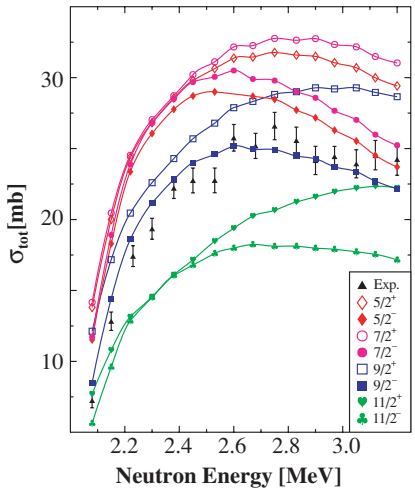

FIG. 6. (Color online) Comparison of the measured level excitation function $\sum_i Y_{\gamma_i}$ for the state at 2000.4 keV with the results of statistical model calculations.

of feeding from higher lying levels and to allow sufficient statistics, the angular distribution measurement taken with $E_n = 2.0$ MeV was used to study states below the 1853 keV level. States above this energy were studied using the results of the $E_n = 3.0$ MeV measurement. The results of nuclear resonance fluorescence (NRF) measurements [25] were also considered. In NRF experiments [34], the nuclei are excited using real photons as a probe. Because of the low-momentum transfer of real photons, this method is selective for states connected to the ground state via $E1$, $M1$, or $E2$ transitions, where $E1$ transitions are favored over the other multipolarities. Therefore, states observed in NRF experiments can only have an angular momentum within a limited range, and these data serve as a cross-check on our assignments.

In Table II, the results obtained in the angular distribution measurements are given together with the results of the excitation functions. The most likely spins were used to calculate the reduced transition probabilities (presented in Table III). Comments explaining these assignments are included in Table II. Here, Lit notes that the literature value was used, AD refers to the respective angular distribution, Exf to the excitation function, DB for the decay behavior, and NRF for information obtained in the NRF measurement [25]. Most spin assignments in Table III are tentative and should be treated with caution. The sequence of the theoretical cross sections for different spins for all states follows that shown in Fig. 6. For higher-lying states the cross sections are reduced due to the increase of the level density with energy. Therefore, a greater number of states with the same angular momentum are competing for the same partial waves.

A close examination of the data presented in Table II reveals that states with a higher excitation energy, for which the spin assignment is based on the excitation function, show a tendency toward $J = 9/2$ and $J = 11/2$. The number of higher-energy $J = 5/2$ or $J = 7/2$ states observed is not as high as expected. It is likely that weak transitions from these states were below the sensitivity limit and not observed, thus the total yields of the levels are too small. Furthermore, the code CINDY requires the level spins as an input to calculate the theoretical cross sections for the inelastic neutron scattering process. To provide this information for the code, the number of levels with an appropriate angular momentum was estimated by applying the particle-core coupling model to the core nucleus ^{140}Ce with the particle in the $d_{5/2}$, $g_{7/2}$, and $h_{11/2}$ subshells. This procedure gave the distribution of possible spins. Couplings of the other two subshells ($d_{3/2}$ and $s_{1/2}$) to the core were neglected. Because the 1608 keV level was strongly excited and the spin is well known, this level was used to normalize the observed yields to the theoretical cross sections.

Because there is no direct measurement, most of the parity assignments are tentative and based on the fact that some states had been previously observed in NRF experiments [25] or on the information given by the excitation functions. The NRF preference for $E1$ excitations led to the assignment of negative parity for most of the states observed with this method. The lifetimes of the observed states were also used as a guide. It was assumed that negative-parity states with the possibility of $E1$ decays depopulate faster and, therefore, have a comparably short lifetime (<100 fs). Further indication was provided by the decay behavior, such as the angular momentum transfer of the transitions. Thus electric multipolarities were favored over magnetic multipolarities.

Table III provides information on the lifetimes determined and the reduced transition probabilities deduced. The errors of the transition energies consist of a fitting part and an energy-dependent systematic part. For the systematic error, the values 200 keV: Δ= 0.1 keV; 2447 keV: Δ=0.5 keV; and 3200 keV: Δ=1.2 keV were assumed to correct for uncertainties in the

TABLE II. Experimental results for the ^{141}Pr levels. Given are the energy of the initial state E_i, the γ-ray energy E_γ, the spin and parity as given in the literature $J^\pi_{\rm lit}$, the result of the angular distribution measurements $J^\pi_{\rm AD}$, the result from the excitation function analysis $J^\pi_{\rm Exf}$, the most likely spin used in a further analysis of the transition rates $J_{{\rm Exp}^\pi}$, and, finally, the source of the spin assignment (Lit = literature, AD = angular distribution, Exf. = excitation function, NRF = seen in previous NRF experiments, DB = decay behavior). For a further discussion, see the text.

E_i (keV)	E_γ (keV)	E_f (keV)	$J^\pi_{\rm lit}$	$J^\pi_{\rm AD}$	$J^\pi_{\rm Exf}$	$J^\pi_{\rm Exp}$	Comment
0			$5/2^+$			$5/2^+$	Lit.
145.445(3)	145.44(20)	0	$7/2^+$			$7/2^+$	Lit.
1117.2(2)	971.75(21)	145.44	$11/2^-$	11/2	$11/2^-$	$11/2^-$	Exp.
	1117.27(28)	0		11/2			
1126.5(2)	981.09(26)	145.44	$3/2^+$	$\leqslant$9/2	$3/2^+$	$3/2^+$	Lit.
	1126.50(21)	0		$\leqslant$9/2			
1292.4(2)	1146.90(22)	145.44	(5/2)+	$\leqslant$9/2	5/2–9/2	$5/2^+$	Lit.
	1292.53(22)	0		$\leqslant$9/2			
1298.4(2)	1298.44(22)	0	$1/2^+$	$\leqslant$7/2	$1/2^+$	$1/2^+$	Exf.
1436.0(3)	309.36(21)	1126.5	$3/2^+$	$\leqslant$7/2	(3/2)	$3/2^+$	Lit.
	1290.67(24)	145.44		$\leqslant$7/2			
	1436.06(26)	0		(7/2)			
1452.1(2)	1306.63(21)	145.44	(7/2)+	7/2,9/2	5/2–9/2	$7/2^+$	Lit.
	1452.20(24)	0		7/2,9/2			
1457.3(2)	339.15(24)	1117.2	$9/2^+$	9/2–13/2	9/2,3/2	$9/2^+$	Exp.
	1311.83(22)	145.44		9/2			
	1457.42(23)	0		9/2,11/2			
1493.9(3)	1348.51(22)	145.44	$11/2^+$	11/2	$11/2^+$	$11/2^+$	Exp.
1520.9(2)	402.87(23)	1117.2	$9/2^+$	9/2–13/2	$9/2^+$	$9/2^+$	Exp.
	1375.56(25)	145.44		9/2			
	1520.98(22)	0		9/2,7/2			
1580.0(3)	287.06(22)	1292.4	$5/2^-$	$\leqslant$9/2	$(5/2^-)$	$5/2^{(-)}$	Lit.
	1434.54(25)	145.44		(11/2)			
	1580.06(25)	0		$\leqslant$9/2	$\leqslant$7/2		
1608.2(3)[a]	1608.20(23)[b]	0	$3/2^+$	$\leqslant$7/2	$3/2^+$	$3/2^+$	Lit.
1651.3(3)	1506.12(30)	145.44	(9/2)+	$\leqslant$11/2	9/2	$7/2^+$	AD 2.0.
	1651.39(23)	0		7/2			
1656.8(3)	358.17(23)	1298.4	$1/2^+$	$\leqslant$5/2	$1/2^+$	$1/2^+$	Exf.
	530.03(21)	1126.5		$\leqslant$5/2			
	1657.51(28)	0		$\leqslant$9/2			
1766.9(3)	273.38(21)	1493.9	$13/2^+$	9/2–13/2	11/2,13/2	$13/2^+$	Exp.
	649.62(21)	1117.2		13/2,9/2			
1786.4(3)	658.78(28)	1126.5	$(5/2^+, 7/2^+)$	$\leqslant$7.2	5/2,7/2	$(5/2, 7/2)^+$	
	1640.93(26)	145.44		$\leqslant$9.2			
	1786.40(25)	0		$\leqslant$9.2			
1796.1(5)	301.91(26)	1493.9	$15/2^+$	(15/2,17/2)	17/2	$15/2^+$	Lit.
1812.4(3)	359.74(22)	1452.1	$(5/2^+)$	(9/2)	5/2–9/2	$9/2^+$	AD 2.0
	1667.13(24)	145.44		9/2			
	1812.65(29)	0		7/2–11/2			
1842.1(3)	384.79(27)	1457.3	$(3/2, 5/2^+)$		5/2–9/2	$7/2^+$	AD 2.0
	389.78(29)	1452.1		$\leqslant$11/2			
	1696.60(27)	145.44		$\leqslant$9/2			
	1842.06(27)	0		7/2			
1853.9(3)	332.66(22)	1520.9	$(7/2^+)$		$11/2^+$	$11/2^+$	AD 2.0
	396.51(25)	1457.3		$\leqslant$13/2			
	1708.65(27)	145.44		11/2			
1975.2(2)	394.52(25)	1580.0	(3/2,5/2/7/2)	$\leqslant$11/2	(3/2)	$3/2^+$	Exf.
	523.03(33)	1452.1		$\leqslant$9/2			
	848.55(29)	1126.5		$\leqslant$7/2			
	1830.04(57)	145.4		$\leqslant$11/2			
	1976.03(45)	0		$\leqslant$9/2			
1985.8(2)	218.67(22)	1766.9	$13/2^+$	11/2–15/2	$13/2^+$	$13/2^+$	Exf.
	465.41(25)	1520.9		$\leqslant$13/2			

TABLE II. *(Continued.)*

E_i (keV)	E_γ (keV)	E_f (keV)	$J^\pi_{\rm lit}$	$J^\pi_{\rm AD}$	$J^\pi_{\rm Exf}$	$J^\pi_{\rm Exp}$	Comment
	868.41(29)	1117.2		7/2–13/2			
1999.8(5)	882.59(21)	1117.2		9/2–13/2	15/2,13/2	$13/2^-$	AD 3.0 & Exf.
2000.4(3)	349.58(25)	1651.3	$9/2^-$		$9/2^-$	$9/2^-$	Exf.
	542.78(26)	1457.3		7/2–13/2			
	548.14(26)	1452.1		5/2–9/2			
	1855.16(60)	145.44		11/2,9/2			
2004.1(2)	545.67(27)	1457.3		7/2–15/2	3/2,9/2,11/2	$11/2^+$	AD 3.0
	1858.20(65)	145.44		11/2			
2017.9(2)	438.27(25)	1580.0		$\leqslant 9/2$	3/2,9/2,11/2	$3/2^+$	Exf.
	719.45(28)	1298.4		$\leqslant 5/2$			
	725.18(32)	1292.4		$\leqslant 11/2$			
	1872.11(41)	145.44		$\leqslant 9/2$			
	2017.53(42)	0		$\leqslant 9/2$			
2045.5(4)	1900.01(22)	145.44		9/2,11/2	$9/2^+$	$9/2^+$	AD 3.0 & Exf.
2075.4(3)	425.19(22)	1651.3		$\leqslant 9/2$	5/2–9/2	5/2,7/2	Exf. & DB
	495.27(22)	1580.0		$\leqslant 9/2$			
	623.02(22)	1452.1		$\leqslant 11/2$			
	782.82(29)	1292.4		$\leqslant 11/2$			
	948.62(30)	1126.5		$\leqslant 7/2$			
	1929.68(43)	145.44		7/2–11/2			
	2075.14(46)	0		$\leqslant 9/2$			
2101.0(3)	664.40(28)	1436.0		$\leqslant 5/2$	$3/2^+$	$3/2^+$	Exf.
	974.36(48)	1126.5		$\leqslant 5/2$			
	2101.99(58)	0		$\leqslant 9/2$			
2104.9(2)	525.28(28)	1580.0	$7/2^-$	$\leqslant 11/2$	$(5/2, 7/2)^-$	$5/2^-, 7/2^-$	
	652.68(27)	1452.1		$\leqslant 11/2$			
	1959.44(42)	145.44		$\leqslant 9/2$			2473 keV
	2104.88(45)	0		$\leqslant 9/2$			
2105.0(4)	987.79(32)	1117.2		9/2–13/2	15/2,17/2	$15/2^-$	
2107.6(5)	311.43(23)	1796.1	$15/2^{(+)}$	13/2–17/2	$15/2^+$	$15/2^+$	AD 3.0 & Exf.
	340.85(25)	1766.9					
2126.2(6)	272.28(22)	1853.9		$\leqslant 15/2$	11/2	$11/2^+$	DB & Exf.
	604.92(28)	1520.9		$\leqslant 13/2$			
	631.77(28)	1493.9		9/2–17/2			
	1008.83(32)	1117.2		13/2			
	1981.43(54)	145.44		$\leqslant 13/2$			
2135.5(2)[d]	678.31(27)	1457.3		$\leqslant 11/2$	$7/2^-, 9/2$	$7/2^-$	DB
	682.89(35)	1452.1		$\leqslant 13/2$			
	1990.04(46)	145.44		7/2–11/2			
	2135.50(45)	0		$\leqslant 9/2$			
2172.1(3)	520.92(26)	1651.3		$\leqslant 11/2$	$9/2^-$	$9/2^-$	AD 3.0 & Exf.
	2026.57(43)	145.44		7/2,9/2			
2188.0(2)	735.98(28)	1452.1		$\leqslant 11/2$	$3/2^+$	$3/2^+$	Exf.
	751.94(29)	1436.0		$\leqslant 7/2$			
	2042.46(47)	145.44		(7/2,9/2)			
	2187.99(55)	0		$\leqslant 9/2$			
2190.6(4)[d]	2044.67(74)	145.44			$1/2^+$	$1/2^-$	Exf.
	2190.76(48)	0		$\leqslant 9/2$			
2206.1(3)	352.73(26)	1853.9			$11/2^+$	$11/2^+$	AD 3.0 & Exf.
	2060.55(43)	145.44		9/2,11/2			
2228.6(2)[d]	386.95(25)	1842.1		$\leqslant 13/2$	$9/2^+$	$5/2, 7/2^+$	DB
	649.0(3)	1580.0					
	776.62(25)	1452.1		$\leqslant 13/2$			
	935.84(34)	1292.4		$\leqslant 11/2$			
	2082.83(45)	145.44		7/2–11/2			
	2228.24(49)	0		7/2–11/2			
2247.5(3)	1120.87(35)	1126.5		$\leqslant 7/2$	5/2,7/2	$5/2^-$	Exf. & NRF
	2247.61(46)	0		$\leqslant 9/2$			

TABLE II. *(Continued.)*

E_i (keV)	E_γ (keV)	E_f (keV)	$J^\pi_{\rm lit}$	$J^\pi_{\rm AD}$	$J^\pi_{\rm Exf}$	$J^\pi_{\rm Exp}$	Comment
2264.3(2)	684.75(31)	1580.0		$\leqslant 9/2$	3/2,9/2,11/2	$3/2^+$	Exf. & DB
	812.38(36)	1452.1		$\leqslant 11/2$			
	828.14(32)	1436.0					
	965.88(38)	1298.4		$\leqslant 7/2$			
	2118.61(45)	145.44		$\leqslant 9/2$			
	2264.02(54)	0		$\leqslant 9/2$			
2267.1(2)	291.65(25)	1975.2			1/2	$1/2^+$	Exf. & DB
	2267.09(28)	0		$\leqslant 9/2$			
2303.7(4)	2158.25(46)	145.44		9/2,11/2	$9/2^+$	$9/2^+$	Exf.
2315.5(3)	1022.90(31)	1292.4		$\leqslant 9/2$	5/2,7/2	$5/2, 7/2^+$	Exf.
	2169.91(50)	145.44		$\leqslant 11/2$			
	2315.67(50)	0		$\leqslant 9/2$			
2336.3(2)	816.03(25)	1520.9		15/2	$15/2^-$	$15/2^-$	AD 3.0 & Exf.
	1218.34(29)	1117.2					
2345.7(2)[d]	558.98(27)	1786.4		$\leqslant 13/2$	3/2,11/2	$7/2^-$	DB
	851.76(23)	1493.9		$\leqslant 15/2$			
	1052.57(34)	1292.4		7/2			
	1229.78(34)	1117.2					
	2199.48(57)	145.44		$\leqslant 11/2$			
	2345.07(56)	0		$\leqslant 9/2$			
2362.8(2)	754.64(24)	1608.2		$\leqslant 7/2$	5/2–9/2	$5/2^-$	Exf. & DB
	1064.38(39)	1298.4		$\leqslant 5/2$			
	1235.67(33)	1126.5		$\leqslant 7/2$			
	2216.99(59)	145.44		$\leqslant 11/2$			
	2362.52(56)	0		$\leqslant 9/2$			
2382.0(3)	861.26(29)	1520.9		7/2–11/2	9/2,11/2	$9/2^-$	Exf.
	1264.51(36)	1117.2		9/2–13/2			
2403.1(3)	945.80(31)	1457.3		7/2–11/2	5/2–9/2	$9/2^+$	
	2257.54(54)	145.44		7/2–11/2			
	2403.20(54)	0		$\leqslant 9/2$			
2419.8(4)	925.92(33)	1493.9		9/2–13/2	5/2–9/2	$9/2^+$	
	2274.21(61)	145.44		9/2			
	2419.90(64)	0		9/2			
2452.9(3)	1326.40(32)	1126.5			$5/2, 7/2^-$	$5/2^-$	Exf. & DB
	2452.65(59)	0		(7/2,9/2)			
2454.1(2)	449.91(22)	2004.1			$15/2^+$	$15/2^+$	Exf.
	687.32(23)	1766.9					
2461.9(3)	810.53(26)	1651.3		(7/2,9/2)	5/2–9/2	5/2,7/2	DB
	1026.24(42)	1436.0		$\leqslant 7/2$			
	1335.04(41)	1126.5		$\leqslant 7/2$			
	2462.20(61)	0		$\leqslant 9/2$			
2473.2(4)[c,d]	368.16(21)	2105.0		$\leqslant 7/2$	1/2,15/2	$1/2^-$	Exf. & DB
2500.2(2)	1046.45(40)	1452.1		9/2	5/2–9/2	$9/2^+$	
	2354.82(29)	145.44		9/2			
2520.1(3)	501.53(28)	2017.9		$7/2, \leq 9/2$	1/2,13/2,11/2	$3/2^+$	DB
	1084.97(40)	1436.0		$\leqslant 9/2$			
	1227.31(44)	1292.4		$\leqslant 11/2$			
	2374.62(70)	145.44		$\leqslant 13/2$			
	2520.70(92)	0		$\leqslant 9/2$			
2563.9(6)	2418.01(89)	145.44		$\leqslant 11/2$	5/2–9/2	$7/2^+$	Exf.
	2564.13(70)	0		9/2,7/2			
2580.8(2)	535.95(28)	2045.5		9/2,11/2,(7/2)	11/2	$11/2^+$	Exf. & DB
	726.73(29)	1853.9		$\leqslant 15/2$			
	1122.88(41)	1457.3		$11/2, \leq 13/2$			
	2435.30(25)	145.44		$9/2, \leq 11/2$			
2583.0(5)[d]	2437.22(77)	145.44		$\leqslant 9/2$	9/2,	$7/2^-$	NRF
	2583.26(72)	0		9/2,7/2			

TABLE II. *(Continued.)*

E_i (keV)	E_γ (keV)	E_f (keV)	$J^\pi_{\rm lit}$	$J^\pi_{\rm AD}$	$J^\pi_{\rm Exf}$	$J^\pi_{\rm Exp}$	Comment
2601.2(5)	2455.74(69)	145.44		$\leqslant 7/2$	3/2–11/2	5/2,7/2	Exf.
	2601.30(84)	0		$\leqslant 11/2$			
2603.8(6)	2458.73(66)	145.44			3/2–11/2	5/2,7/2	Exf.
	2603.07(83)	0		$\leqslant 11/2$			
2607.1(8)	2607.06(76)	0		$\leqslant 9/2$	$1/2^+$	$1/2^+$	Exf.
2611.7(5)	1318.59(46)	1292.4		$\leqslant 9/2$	$9/2^+$	$9/2^+$	Exf.
	2612.42(72)	0		$\leqslant 9/2$			
2623.2(4)	1330.33(45)	1292.4		$\leqslant 11/2$	3/2–9/2	7/2	AD 3.0
	2477.72(67)	145.44		$\leqslant 11/2$			
	2623.81(75)	0		7/2,9/2			
2646.5(5)	2500.60(69)	145.44		7/2,9/2,11/2	3/2–11/2	$9/2^+$	NRF
	2646.91(75)	0		7/2,9/2,11/2			
2659.6(8)[3]	2514.14(75)	145.44		11/2,(9/2,13/2)	1/2,15/2	$11/2^+$	AD 3.0
2668.8(3)	1175.16(32)	1493.9		$>9/2$	11/2,13/2	$13/2^-$	Exf. & DB
	1216.36(43)	1452.1		11/2,13/2			
	1551.26(42)	1117.2		15/2,(11/2)			
2682.9(4)	870.93(41)	1812.4		$\leqslant 13/2$	5/2,7/2	$(5/2, 7/2)^+$	
	1246.08(54)	1436.0		$\leqslant 9/2$			
	1556.27(41)	1126.5		$\leqslant 7/2$			
	2537.5(11)	145.44		$\leqslant 9/2$			
	2683.24(79)	0		$\leqslant 9/2$			
2707.4(4)	1590.16(35)	1117.2			$15/2^-$	$15/2^-$	Exf.
2709.8(4)	1411.33(32)	1298.4			3/2	$3/2^+$	
	1583.28(43)	1126.5		$\leqslant 7/2$			
2718.4(4)	1197.53(36)	1520.9		7/2–13/2	9/2,11/2	9/2,11/2	
	1601.07(53)	1117.2		$\leqslant 15/2$			
2722.0(4)	1271.60(48)	1452.1			3/2,	$3/2^+$	Exf. & DB
	1422.39(58)	1298.4					
	2576.04(88)	145.44		$\leqslant 11/2$			
	2721.48(82)	0		$\leqslant 9/2$			
2731.5(4)	877.51(42)	1853.9			9/2,	$9/2^+$	Exf. & DB
	1278.65(45)	1452.1					
	2586.62(83)	145.44		$\leqslant 11/2$			
	2732.12(84)	0		$\leqslant 11/2$			
2739.7(3)	1159.62(27)	1580.0			1/2,	$1/2^-$	Exf. & DB
2777.5(5)	923.77(37)	1853.9			5/2–9/2	9/2	AD 3.0
	2631.89(78)	145.44		9/2			
2781.8(6)	2637.37(81)	145.44			13/2,	$13/2^+$	Exf. & DB
	781.84(89)	0		7/2–11/2			
2782.3(8)	576.93(25)	2206.1		$7/2, \leqslant 11/2$	5/2,7/2	$(5/2, 7/2)^+$	Exf+n.o.NRF
	1261.13(54)	1520.9		$\leqslant 9/2$			
2801.7(3)	1151.18(46)	1651.3			3/2,9/2,11/2	$9/2^+$	Exf. & DB
	2655.96(37)	145.44		$\leqslant 11/2$			
	2801.76(27)	0		$\leqslant 9/2$			
2807.1(3)	491.37(34)	2315.5			3/2,9/2,11/2	$3/2^+$	
	2661.96(42)	145.44		$\leqslant 13/2$			
	2807.13(22)	0		$\leqslant 9/2$			
2811.0(3)	1201.08(45)	1608.2		$\leqslant 7/2$	$1/2^{(+)}$	$1/2^+$	Exf.
	2810.95(23)	0					
2813.9(3)	1233.07(36)	1580.0			$1/2^{(-)}$	$1/2^-$	Exf.
	1687.70(34)	1126.5		$\leqslant 5/2$			
2837.4(8)	2691.97(94)	145.44		9/2	3/2–11/2	$(5/2,7/2)^-$	AD 3.0
	2837.5(11)	0		$\leqslant 11/2$			& NRF
2839.6(3)	2694.17(39)	145.44		$\leqslant 13/2$	3/2,9/2,11/2	3/2,9/2,11/2	
2845.1(5)	1186.83(48)	1656.8		$\leqslant 7/2$	3/2,	$3/2^-$	Exf. & NRF
	1546.60(59)	1298.4					
	2846.2(11)	0		$\leqslant 9/2$			

TABLE II. *(Continued.)*

E_i (keV)	E_γ (keV)	E_f (keV)	$J^\pi_{\rm lit}$	$J^\pi_{\rm AD}$	$J^\pi_{\rm Exf}$	$J^\pi_{\rm Exp}$	Comment
2847.5(4)	1005.00(36)	1842.1		9/2	5/2–9/2	$9/2^+$	AD 3.0 & DB
	1353.97(54)	1493.9					
	1389.89(57)	1457.3					
	2702.8(12)	145.44		$\leqslant 11/2$			
	2848.4(11)	0					
2863.1(8)[d]	1570.93(56)	1292.4			(15/2)		
	2716.8(15)	145.44					
2881.7(5)[d]	1028.04(46)	1853.9			9/2,11/2,(3/2)	$7/2, 9/2^+$	DB
	1424.45(78)	1457.3					
	1428.46(62)	1452.1					
	2737.0(16)	145.44					
	2882.3(11)	0					
2887.5(4)	1075.23(53)	1812.4			9/2,11/2	9/2,11/2	Exf. & DB
	1366.96(38)	1520.9					
	1392.82(52)	1493.9					
	1769.60(56)	1117.2					
	2742.5(17)	145.44					
2897.1(8)	438.97(78)	1457.3			13/2,11/2	$11/2^+$	Exf. & DB
	2752.04(95)	145.44					
2929.2(5)	1635.97(48)	1292.4			5/2,7/2	5/2,7/2	
	2785.2(11)	145.44					
	2930.3(12)	0					
2941.4(8)[d]	1484.2(10)	1457.3			1/2,3/2,11/2		
	1488.55(76)	1452.1					
	2796.4(14)	145.44					
	2941.7(14)	0					
2950.3(9)	1514.40(64)	1436.0			1/2	$1/2^+$	Exf. & DB
	2950.1(17)	0					
2983.0(3)	2839.0(7)	145.4			3/2–11/2	3/2	DB & NRF
	2983.04(46)	0					
3000.7(3)	955.95(42)	2045.5			11/2,13/2	$11/2^+$	Exf. & DB
	1479.49(51)	1520.9					
	2855.20(26)	145.44					
3016.0(8)	940.96(47)	2075.4			1/2–11/2	$5/2^-$	DB & NRF
	1887.9(13)	1126.5					
	2871.0(19)	145.44					
	3015.9(15)	0					
3034.1(8)	1734.94(69)	1298.4			1/2,	$1/2^+$	Exf. & DB
	1742.49(76)	1292.4					
3045.6(8)	1524.57(66)	1520.9			11/2,9/2	$11/2^+, 9/2$	
	2900.2(12)	145.44					
3064.2(7)	960.45(59)	2104.9			11/2,9/2	$11/2^+, 9/2$	
	1209.90(55)	1853.9					
	2918.4(12)	145.44					

[a]State used to normalize the excitation function yields.
[b]Transition used to normalize the angular distribution data.
[c]State tentatively assigned.
[d]State possibly deexcited by unobserved transitions.

extrapolation to the energy region above the 2447 keV γ ray for which ^{226}Ra does not provide calibration points.

The $F(\tau)$ value derived from the angular distribution data led to the level lifetimes. For states only weakly excited or with a lifetime close to or longer than 1 ps, only lower limits could be given. Multipole-mixing ratios are given using the convention of Ref. [35]. The reduced transition probabilities $B(\Pi L)\downarrow$ were calculated using the standard formulas. Internal conversion coefficients were not considered, as they give only small corrections compared to the relatively large experimental errors. If only a lower limit for the lifetime was obtained, the upper limit for the $B(\Pi L)\downarrow$ value is given. For cases of parity-conserving transitions where no multipole-mixing ratio could be measured, both possible reduced transition probabilities are

TABLE III. Experimental lifetimes and calculated reduced transition probabilities. Given are the level energies, the most probable spins (see discussion in the text), the observed transition energies, the spins of the final levels, the attenuation factors $F(\tau)$, the resulting lifetimes τ, the multipole-mixing ratios δ, the observed transition intensities I_γ, and the calculated transition probabilities $B(\Pi L)\downarrow$. The limits of the $B(\Pi L)\downarrow$ values consist of the upper errors added to the measured values.

E_i (keV)	J_i^π	E_γ (keV)	E_f (keV)	J_f^π	$F(\tau)$	τ (fs)	I_γ (%)	δ or πL	$B(E1)\downarrow$ (10^{-3} W.u.)	$B(M1)\downarrow$ (μ_N^2)	$B(E2)\downarrow$ (W.u.)
0	$5/2^+$										
145.445(3)	$7/2^+$	145.44(20)	0	$5/2^+$	0.000(27)	>1780	100	$E2+M1$			
1117.2(2)	$11/2^-$	971.75(21)	145.44	$7/2^+$	0.000(40)	>1090	89.8(3)	$-0.170^{0.075}_{0.087}$			
								$-11.5^{5.8}_{-\infty}$			
		1117.27(28)	0	$5/2^+$			10.2(3)	$E3$			
1126.5(2)	$3/2^+$	981.09(26)	145.44	$7/2^+$	0.062(83)	>271	2.7(1)	$E2$			$\leqslant 2.15$
		1126.50(21)	0	$5/2^+$			97.3(1)	0.47(6)[a]		$\leqslant 0.0132$	$\leqslant 7.7$
1292.4(2)	$5/2^+$	1146.90(22)	145.44	$7/2^+$	0.086(19)	480^{150}_{95}	40.0(5)	$E2+M1$		$\leqslant 0.0039$	$\leqslant 9.0$
		1292.53(22)	0	$5/2^+$			60.0(5)	$E2+M1$		$\leqslant 0.0042$	$\leqslant 8.2$
1298.4(2)	$1/2^+$	1298.44(22)	0	$5/2^+$	0.085(32)	485^{315}_{145}	100	$E2$			$10.6^{4.5}_{2.4}$
1436.0(3)	$3/2^+$	309.36(21)	1126.5	$3/2^+$	0.120(28)	330^{115}_{70}	1.5(8)	$E2+M1$		$\leqslant 0.016$	$\leqslant 549$
		1290.67(24)	145.44	$7/2^+$			52.4(8)	$E2$			$8.4^{2.4}_{1.6}$
		1436.06(26)	0	$5/2^+$			46.1(8)	$E2+M1$		$\leqslant 0.0035$	$\leqslant 5.6$
1452.1(2)	$7/2^+$	1306.63(21)	145.44	$7/2^+$	0.090(22)	450^{160}_{100}	81.6(4)	$-0.90^{0.20}_{0.31}$		$0.0026^{0.0014}_{0.0012}$	$4.00^{2.82}_{1.57}$
								$28.9^{5.7}_{7.0}$		$<10^{-4}$	$9.0^{2.5}_{1.6}$
		1452.20(24)	0	$5/2^+$			18.4(4)	$5.1^{5.5}_{2.0}$		$<10^{-4}$	$1.2^{0.4}_{0.3}$
								$0.48^{0.26}_{0.12}$		$0.0006^{0.0003}_{0.0002}$	$0.22^{0.22}_{0.12}$
1457.3(2)	$9/2^+$	339.15(24)	1117.2	$11/2^-$	0.108(21)	370^{100}_{70}	0.9(1)	$E1$	0.23(0.7)		
		1311.83(22)	145.44	$7/2^+$			73.4(4)	$0.053^{0.026}_{0.022}$		0.0050(11)	$0.03^{0.05}_{0.02}$
								$-8.9^{1.9}_{1.7}$		0.0001(1)	$9.6^{2.2}_{1.6}$
		1457.42(23)	0	$5/2^+$			25.7(4)	$E2$			$2.0^{0.5}_{0.4}$
1493.9(3)	$11/2^+$	1348.51(22)	145.44	$7/2^+$	0.063(27)	660^{515}_{210}	100	$E2$			$6.4^{2.9}_{1.5}$
1520.9(2)	$9/2^+$	402.87(23)	1117.2	$11/2^-$	0.170(17)	217^{27}_{23}	1.8(1)	$E1$	0.46(8)		
		1375.56(25)	145.44	$7/2^+$			10.3(3)	$-0.26^{0.11}_{0.13}$		0.001(2)	$0.12^{0.16}_{0.08}$
								$-2.2^{0.5}_{0.7}$	0.0002(1)		$1.5^{0.4}_{0.3}$
		1520.98(22)	0	$5/2^+$			87.9(3)	$E2$			$9.4^{1.1}_{0.9}$
1580.0(3)	$5/2^{(-)}$	287.06(22)	1292.4	$5/2^+$	0.121(24)	320^{90}_{60}	2.2(1)	$E1$	1.05(28)		
		1434.54(25)	145.44	$7/2^+$			72.0(5)	$E1$	0.28(6)		
		1580.06(25)	0	$5/2^+$			25.8(5)	$E1$	0.074(8)		
1608.2(3)	$3/2^+$	1608.20(23)	0	$5/2^+$	0.739(17)	17^1_1	100	$E2+M1$		$\leqslant 0.0854$	$\leqslant 109.5$
1651.3(3)	$7/2^+$	1506.12(30)	145.44	$7/2^+$	0.187(23)	190^{30}_{25}	7.9(2)	$0.232^{0.059}_{0.057}$		0.0007(1)	0.05(4)
								$16.7^{\infty}_{8.8}$		$<10^{-4}$	$1.00^{0.18}_{0.15}$
		1651.39(23)	0	$5/2^+$			92.1(2)	$E2$			$7.4^{1.1}_{0.9}$
1656.8(3)	$1/2^+$	358.17(23)	1298.4	$5/2^+$	0.012(31)	>970	7.9(4)	$E2$			$\leqslant 273$
		530.03(21)	1126.5	$3/2^+$			47.5(8)			$\leqslant 0.0195$	$\leqslant 224$
		1657.51(28)	0	$5/2^+$			44.6(8)	$E2$			$\leqslant 0.70$
1766.9(3)	$13/2^+$	273.38(21)	1493.9	$11/2^+$	0.032(42)	>540	18.8(7)	$0.069^{0.073}_{0.081}$		$\leqslant 0.101$	$\leqslant 21.2$
		649.62(21)[b]	1117.2	$11/2^-$			81.2(7)	$E1$	$\leqslant 1.999$		
1786.4(3)	(5/2,	658.78(28)	1126.5	$3/2^+$	0.139(27)	270^{75}_{50}	3.2(2)	$E2+M1$		$\leqslant 0.0031$	$\leqslant 23$
	$7/2)^+$	1640.93(26)	145.44	$7/2^+$			30.8(6)	$E2+M1$		$\leqslant 0.0019$	$\leqslant 2.3$
		1786.40(25)	0	$5/2^+$			66.0(7)	$E2+M1$		$\leqslant 0.0031$	$\leqslant 3.1$
1796.1(5)	$15/2^+$	301.91(26)	1493.9	$11/2^+$	0.000(755)	>15	100	$E2$			
1812.4(3)	$9/2^+$	359.74(22)	1452.1	$(7/2)^+$	0.035(21)	1170^{1760}_{450}	9.1(4)	$-0.107^{0.130}_{0.133}$		0.010(7)	$2.8^{18.9}_{2.8}$
								$-3.5^{1.2}_{2.8}$		$0.0007^{0.0018}_{0.0006}$	225^{170}_{87}
		1667.13(24)	145.44	$7/2^+$			59.5(8)	$-0.248^{0.041}_{0.043}$		0.0006(4)	$0.04^{0.05}_{0.02}$
								$-2.29^{0.25}_{0.36}$		0.0001(1)	$0.63^{0.44}_{0.20}$
		1812.65(29)	0	$5/2^+$			31.4(7)	$E2$			$0.26^{0.17}_{0.26}$

TABLE III. *(Continued.)*

E_i (keV)	J_i^π	E_γ (keV)	E_f (keV)	J_f^π	$F(\tau)$	τ (fs)	I_γ (%)	δ or πL	$B(E1)\downarrow$ (10^{-3} W.u.)	$B(M1)\downarrow$ (μ_N^2)	$B(E2)\downarrow$ (W.u.)
1842.1(3)	$7/2^+$	384.79(27)	1457.3	$9/2^+$	0.041(18)	1010^{850}_{320}	1.2(2)	$E2+M1$		$\leqslant 0.0019$	$\leqslant 44$
		389.78(29)	1452.1	$(7/2)^+$			0.9(2)	$E2+M1$		$\leqslant 0.0015$	$\leqslant 32$
		1696.60(27)	145.44	$7/2^+$			34.6(7)	$-0.52^{0.21}_{0.28}$		$0.0003(2)$	$0.10^{0.12}_{0.07}$
								$2.8^{4.2}_{1.1}$		$<10^{-4}$	$0.41^{0.26}_{0.15}$
		1842.06(27)	0	$5/2^+$			63.4(7)	$0.57^{0.23}_{0.16}$		$0.0004(3)$	$0.14^{0.17}_{0.08}$
								$4.6^{4.4}_{1.7}$		$<10^{-4}$	$0.44^{0.34}_{0.06}$
1853.9(3)	$11/2^+$	332.66(22)	1520.9	$9/2^+$	0.038(25)	1090^{2260}_{460}	1(1)	$E2+M1$		$\leqslant 0.0039$	$\leqslant 115$
		396.51(25)	1457.3	$9/2^+$			5.9(4)	$0.313^{0.158}_{0.138}$		$0.0045^{0.0041}_{0.0035}$	$9.3^{24.0}_{7.7}$
								$5.2^{10.7}_{2.2}$		$0.0002^{0.0007}_{0.0002}$	100^{86}_{42}
		1708.65(27)	145.44	$7/2^+$			93.8(4)	$E2$			$1.1^{0.8}_{0.3}$
1975.2(2)	$3/2^+$	394.52(25)	1580.0	$5/2^{(-)}$	0.079(25)	560^{270}_{145}	1.5(5)	$E1$	$0.16^{0.11}_{0.10}$		
		523.03(33)	1452.1	$(7/2)^+$			6.9(4)	$E2$			60^{24}_{23}
		848.55(29)	1126.5	$3/2^+$			27.0(7)	$E2+M1$		$\leqslant 0.0062$	$\leqslant 28.5$
		1830.04(57)	145.4	$7/2^+$			23.6(6)	$E2$			0.39(14)
		1976.03(45)	0	$5/2^+$			41.0(8)	$E2+M1$		$\leqslant 0.0007$	$\leqslant 0.63$
1985.8(2)	$13/2^+$	218.67(22)	1766.9	$13/2^+$	0.021(53)	>600	6.1(8)	$E2+M1$		$\leqslant 0.062$	$\leqslant 4321$
		465.41(25)	1520.9	$9/2^+$			12.2(8)	$E2$			$\leqslant 187$
		868.41(29)	1117.2	$11/2^-$			81.8(11)	$E1$	$\leqslant 0.757$		
1999.8(5)	$13/2^-$	882.59(21)	1117.2	$11/2^-$	0.202(83)	190^{165}_{70}	100	$-0.013^{0.044}_{0.617}$		$0.043^{0.024}_{0.020}$	$0.03^{1.10}_{0.03}$
								$-9.9^{3.6}_{11.3}$		$0.0004^{0.0012}_{0.0004}$	182^{104}_{85}
2000.4(3)	$9/2^-$	349.58(25)	1651.3	$9/2^+$	0.132(43)	315^{175}_{90}	2.3(2)	$E1$	0.62(56)		
		542.78(26)	1457.3	$9/2^+$			3.4(2)	$E1$	0.24(18)		
		548.14(26)	1452.1	$7/2^+$			19.3(16)	$E1$	$1.34^{0.62}_{0.58}$		
		1855.16(60)	145.44	$7/2^+$			75.0(2)	$E1$	0.134(55)		
2004.1(2)	$11/2^+$	545.67(27)	1457.3	$9/2^+$	0.043(25)	1060^{1460}_{400}	3(3)	$0.40^{0.21}_{0.19}$		$0.0009(8)$	$1.5^{4.5}_{1.5}$
								$4.1^{8.6}_{2.0}$		$0.0001^{0.0003}_{0.0001}$	$10.4^{8.2}_{7.7}$
		1858.20(65)	145.44	$7/2^+$			97.0(3)	$E2$			0.78(47)
2017.9(2)	$3/2^+$	438.27(25)	1580.0	$5/2^{(-)}$	0.076(29)	580^{380}_{170}	4.8(4)	$E1$	0.36(18)		
		719.45(28)	1298.4	$1/2^+$			8.8(6)	$E2+M1$		$\leqslant 0.0034$	$\leqslant 22.2$
		725.18(32)	1292.4	$5/2^+$			2.8(5)	$E2+M1$		$\leqslant 0.0011$	$\leqslant 7.3$
		1872.11(41)	145.44	$7/2^+$			28.4(8)	$E2$			0.40(18)
		2017.53(42)	0	$5/2^+$			55.2(9)	$E2+M1$		$\leqslant 0.001$	$\leqslant 0.78$
2045.5(4)	$9/2^+$	1900.01(22)	145.44	$7/2^+$	0.046(25)	980^{1240}_{360}	100	$0.492^{0.078}_{0.059}$		$0.0007(4)$	$0.15^{0.15}_{0.10}$
								$3.4^{0.8}_{0.6}$		$0.0001(1)$	$0.71^{0.45}_{0.41}$
2075.4(3)	5/2,	425.19(22)	1651.3	$7/2, 9/2^+$	0.135(37)	310^{135}_{80}	2.7(4)	$E2+M1$		$\leqslant 0.0096$	$\leqslant 176$
	$7/2^+$	495.27(22)	1580.0	$5/2^{(-)}$			4.5(4)	$E1$	0.43(18)		
		623.02(22)	1452.1	$7/2^+$			6.5(5)	$E2+M1$		$\leqslant 0.007$	$\leqslant 59$
		782.82(29)	1292.4	$5/2^+$			12.3(6)	$E2+M1$		$\leqslant 0.0065$	$\leqslant 35.2$
		948.62(30)	1126.5	$3/2^+$			38.3(8)	$E2+M1$		$\leqslant 0.011$	$\leqslant 42$
		1929.68(43)	145.44	$7/2^+$			21.6(7)	$E2+M1$		$\leqslant 0.0008$	$\leqslant 0.67$
		2075.14(46)	0	$5/2^+$			14.1(6)	$E2+M1$		$\leqslant 0.0004$	$\leqslant 0.30$
2101.0(3)	$3/2^+$	664.40(28)	1436.0	$3/2^+$	0.166(45)	240^{105}_{60}	10.8(6)	$E2+M1$		$\leqslant 0.012$	$\leqslant 90$
		974.36(48)	1126.5	$3/2^+$			78.6(11)	$E2+M1$		$\leqslant 0.027$	$\leqslant 94$
		2101.99(58)	0	$5/2^+$			10.6(10)	$E2+M1$		$\leqslant 0.0004$	$\leqslant 0.29$
2104.9(2)	$5/2^-$	525.28(28)	1580.0	$5/2^{(-)}$	0.28(3)	125^{21}_{16}	4.1(5)	$E2+M1$		$\leqslant 0.017$	$\leqslant 197$
		652.68(27)	1452.1	$7/2^+$			12.4(5)	$E1$	1.28(24)		
		1959.44(42)	145.44	$7/2^+$			49.8(9)	$E1$	0.19(3)		
		2104.88(45)	0	$5/2^+$			33.6(9)	$E1$	0.104(18)		
2105.0(4)	$15/2^-$	987.79(32)	1117.2	$11/2^-$	0.181(131)	220^{700}_{110}	100	$E2$			92^{95}_{70}
2107.6(5)	$15/2^+$	311.43(23)	1796.1	$15/2^+$	0.213(337)	>41	65.2(25)	$E2+M1$		<3.1	<106200
		340.85(25)	1766.9	$13/2^+$			34.8(25)	$E2+M1$		<1.3	<37200

TABLE III. *(Continued.)*

E_i (keV)	J_i^π	E_γ (keV)	E_f (keV)	J_f^π	$F(\tau)$	τ (fs)	I_γ (%)	δ or πL	$B(E1)\downarrow$ (10^{-3} W.u.)	$B(M1)\downarrow$ (μ_N^2)	$B(E2)\downarrow$ (W.u.)
2126.2(6)	$11/2^+$	272.28(22)	1853.9	$11/2^+$	0.047(181)	>164	18.1(24)	$E2+M1$		<0.55	<24600
		604.92(28)	1520.9	$9/2^+$			11.0(12)	$E2+M1$		<0.031	<273
		631.77(28)	1493.9	$11/2^+$			11.4(11)	$E2+M1$		<0.027	<226
		669[c]	1457.3	$9/2^+$			24.5	$E2+M1$		<0.049	<365
		1008.83(32)	1117.2	$11/2^-$			26.6(17)	$E1$	<0.97		
		1981.43(54)	145.44	$7/2^+$			8.4(11)	$E2$			<0.55
2135.5(2)	$7/2^-$	678.31(27)	1457.3	$9/2^+$	0.11(3)	385^{165}_{95}	16.2(6)	$E1$	0.49(17)		
		682.89(35)	1452.1	$7/2^+$			3.0(6)	$E1$	0.088(45)		
		1990.04(46)	145.44	$7/2^+$			21.2(8)	$E1$	0.025(9)		
		2135.50(45)	0	$5/2^+$			59.6(10)	$E1$	0.057(19)		
2172.1(3)	$9/2^-$	520.92(26)	1651.3	$9/2^+$	0.25(3)	145^{26}_{21}	8.0(6)	$E1$	1.41(34)		
		2026.57(43)	145.44	$7/2^+$			92.0(6)	$E1$	0.274(48)		
2188.0(2)	$3/2^+$	735.98(28)	1452.1	$7/2^+$	0.113(51)	375^{345}_{130}	25.3(11)	$E2$			59(34)
		751.94(29)	1436.0	$3/2^+$			19.8(9)	$E2+M1$		⩽0.011	⩽66
		2042.46(47)	145.44	$7/2^+$			41.3(12)	$E2$			0.59(33)
		2187.99(55)	0	$5/2^+$			13.6(13)	$E2+M1$		⩽0.0003	⩽0.23
2190.6(4)	$1/2^-$	2044.67(74)	145.44	$7/2^+$	0.067(64)	>310	6.5(27)	$E3$			
		2190.76(48)	0	$5/2^+$			93.5(27)	$M2$			
2206.1(3)	$11/2^+$	352.73(26)	1853.9	$11/2^+$	0.162(27)	246^{57}_{41}	3.4(7)	$E2+M1$			
		2060.55(43)	145.44	$7/2^+$			96.6(7)	$E2$			
2228.6(2)	$7/2^+$	386.95(25)	1842.1	$7/2^+$	0.043(39)	1040^{8800}_{510}	3.9(8)	$E2+M1$		⩽0.008	⩽177
		649.0(3)[b]	1580.0	$5/2^-$			44(16)	$E1$	$0.558^{0.737}_{0.699}$		
		776.62(25)	1452.1	$7/2^+$			3.5(7)	$E2+M1$		⩽0.0009	⩽4.9
		935.84(34)	1292.4	$5/2^+$			3.5(8)	$E2+M1$		⩽0.0005	⩽1.9
		2082.83(45)	145.44	$7/2^+$			22.9(12)	$0.37^{0.12}_{0.11}$		0.0001(1)	$0.01^{0.03}_{0.01}$
								$5.333^{5.255}_{2.083}$		$<10^{-4}$	0.10(11)
		2228.24(49)	0	$5/2^+$			16.7(11)	$E2+M1$		⩽0.0002	⩽0.12
2247.5(3)	$5/2^-$	1120.87(35)	1126.5	$3/2^+$	0.184(30)	212^{50}_{36}	11.1(16)	$E1$	0.134(47)		
		2247.61(46)	0	$5/2^+$			88.9(16)	$E1$	0.133(30)		
2264.3(2)	$3/2^+$	684.75(31)	1580.0	$5/2^-$	0.157(52)	260^{150}_{80}	5.9(11)	$E1$	0.26(15)		
		812.38(36)	1452.1	$7/2^+$			4.8(14)	$E2$			$9.99^{7.0}_{6.6}$
		828.14(32)	1436.0	$3/2^+$			9(2)	$E2+M1$		⩽0.0057	⩽28
		965.88(38)	1298.4	$5/2^+$			8.5(13)	$E2+M1$		⩽0.0033	⩽11.6
		2118.61(45)	145.44	$7/2^+$			49.1(18)	$E2$			0.85(38)
		2264.02(54)	0	$5/2^+$			24.2(17)	$E2+M1$		⩽0.0007	⩽0.44
2267.1(2)	$1/2^+$	291.65(25)	1975.2	$3/2^+$		>265	6.3(50)	$E2+M1$		<0.097	<3795
		2267.09(28)	0	$5/2^+$			93.7(50)	$E2$			<1.17
2303.7(4)	$9/2^+$	2158.25(46)	145.44	$7/2^+$	0.116(40)	360^{210}_{105}	100	$0.16^{0.23}_{0.31}$		0.0015(7)	$0.06^{0.08}_{0.04}$
								$18.7^{\infty}_{10.8}$		$<10^{-4}$	1.11(42)
2315.5(3)	5/2	1022.90(31)	1292.43	$5/2^+$	0.202(36)	188^{51}_{35}	40.(12)	$E2+M1$		⩽0.0145	⩽45.9
	$7/2^+$	2169.91(50)	145.44	$7/2^+$			16.6(8)	$E2+M1$		⩽0.0006	⩽0.45
		2315.67(50)	0	$5/2^+$			42.6(13)			⩽0.0013	⩽0.81
2336.3(2)	$(15/2^-)$	816.03(25)	1520.9	$9/2^+$	0.230(321)	>40	44.5(57)	$E3$			
		1218.34(29)	1117.2	$11/2^-$			55.5(57)	$E2$			<105
2345.7(2)	$9/2^+$	558.98(27)	1786.4	$(5/2,7/2)^+$	0.134(69)	305^{370}_{120}	12.8(10)			⩽0.024	⩽248
		851.76(23)	1493.9	$11/2^+$			16.6(11)	$E2+M1$		⩽0.0085	⩽39
		1052.57(34)	1292.4	$5/2^+$			22.6(13)	$E2$			10.8(74)
		1229.78(34)	1117.2	$11/2^-$			9.2(18)	$E1$	0.058(48)		
		2199.48(57)	145.44	$7/2^+$			13.8(12)	$E2+M1$		⩽0.0004	⩽0.29
		2345.07(56)	0	$5/2^+$			25.0(14)	$E2$			0.22(15)
2362.8(2)	$5/2^-$	754.64(24)	1608.2	$3/2^+$	0.468(60)	56^{15}_{12}	9.4(8)	$E1$	1.41(50)		

TABLE III. *(Continued.)*

E_i (keV)	J_i^π	E_γ (keV)	E_f (keV)	J_f^π	$F(\tau)$	τ (fs)	I_γ (%)	δ or πL	$B(E1)\downarrow$ (10^{-3} W.u.)	$B(M1)\downarrow$ (μ_N^2)	$B(E2)\downarrow$ (W.u.)
		1064.38(39)	1298.4	$5/2^+$			8.8(15)	$E1$	0.47(21)		
		1235.67(33)	1126.5	$3/2^+$			57.2(17)	$E1$	1.95(59)		
		2216.99(59)	145.44	$7/2^+$			7.1(8)	$E1$	0.042(16)		
		2362.52(56)	0	$5/2^+$			17.5(11)	$E1$	0.085(29)		
2382.0(3)	$9/2^-$	861.26(29)	1520.9	$9/2^+$	0.118(59)	350^{400}_{130}	72.4(12)	$E1$	1.16(72)		
		1264.51(36)	1117.2	$11/2^-$			27.6(12)	$E2+M1$		$\leqslant$0.0036	$\leqslant$7.5
2403.1(3)	$9/2^+$	945.80(31)	1457.3	$9/2^+$	0.062(38)	710^{1230}_{290}	25.7(11)	$E2+M1$		$\leqslant$0.0042	$\leqslant$15.6
		2257.54(54)	145.44	$7/2^+$			14.7(10)	$0.40^{0.41}_{0.22}$		0.0001(1)	$0.01^{0.04}_{0.01}$
								$4.8^{\infty}_{3.0}$		$<10^{-4}$	$0.06^{0.07}_{0.05}$
		2403.20(54)	0	$5/2^+$			59.5(14)	$E2$			$0.20^{0.14}_{0.20}$
2419.8(4)	$9/2^+$	925.92(33)	1493.9	$11/2^+$	0.065(50)	675^{2500}_{314}	18.7(19)	$E2+M1$		$\leqslant$0.0039	$\leqslant$15.2
		2274.21(61)	145.44	$7/2^+$			48.2(42)	$-0.42^{0.18}_{1.99}$		0.0003(3)	$0.03^{0.32}_{0.03}$
								$-1.6^{1.3}_{0.8}$		$0.0001^{0.0005}_{0.0001}$	$0.16^{0.21}_{0.17}$
		2419.90(64)	0	$5/2^+$			33.2(55)	$E2$			0.11(12)
2452.9(3)	$5/2^-$	1326.40(32)	1126.5	$3/2^+$	0.653(42)	27^5_4	8(7)	$E1$	0.46(48)		
		2452.65(59)	0	$5/2^+$			92(7)	$E1$	0.83(21)		
2454.1(2)	$15/2^+$	449.91(22)	2004.1	$11/2^+$	0.000(259)	$>$135	38.6(32)	$E2$			$<$3143
		687.32(23)	1766.9	$13/2^+$			61.4(32)	$0.26^{0.15}_{0.14}$		$<$0.082	$<$83
2461.9(3)	$5/2^+$	810.53(26)	1651.3	$7/2^+$	0.194(49)	196^{82}_{48}	13.7(13)	$E2+M1$		$\leqslant$0.012	$\leqslant$54
		1026.24(42)	1436.0	$3/2^+$			12.6(12)	$E2+M1$		$\leqslant$0.0048	$\leqslant$15.1
		1335.04(41)	1126.5	$3/2^+$			14.6(12)	$E2+M1$		$\leqslant$0.0025	$\leqslant$4.7
		2462.20(61)	0	$5/2^+$			59.2(19)	$E2+M1$		$\leqslant$0.0016	$\leqslant$0.85
2473.2(4)	$1/2^-$	368.16(21)	2105.0	$5/2^-$	0.222(496)	$>$20	100	$E2$			$<$18957
2500.2(2)	$9/2^+$	1046.45(40)	1452.1	$7/2^+$	0.244(42)	147^{40}_{28}	16.4(12)	$-0.24^{0.22}_{0.47}$		$0.0052^{0.0020}_{0.0027}$	$0.9^{60}_{0.9}$
								$-2.4^{1.3}_{2.9}$		$0.0008^{0.0025}_{0.0008}$	$14.19^{6.82}_{8.43}$
		2354.82(29)	145.44	$7/2^+$			83.6(12)	$-0.064^{0.084}_{0.078}$		0.0025(6)	$0.01^{0.03}_{0.01}$
								$-4.1^{1.1}_{1.6}$		0.0001(2)	1.40(40)
2520.1(3)	$3/2^+$	501.53(28)	2017.9	$3/2^+$	0.148(132)	270^{2550}_{150}	16.1(22)	$E2+M1$		$\leqslant$0.064	$\leqslant$839
		1084.97(40)	1436.0	$3/2^+$			18.8(29)	$E2+M1$		$\leqslant$0.0074	$\leqslant$20.8
		1227.31(44)	1292.4	$5/2^+$			19.8(27)	$E2+M1$		$\leqslant$0.0054	$\leqslant$11.8
		2374.62(70)	145.44	$7/2^+$			25.8(27)	$E2$			$0.24^{0.32}_{0.24}$
		2520.70(92)	0	$5/2^+$			19.5(25)	$E2+M1$		$\leqslant$0.0006	$\leqslant$0.31
2563.9(6)	$7/2^-$	2418.01(89)	145.44	$7/2^+$	0.375(40)	79^{15}_{12}	33.0(47)	$E1$	0.106(34)		
		2564.13(70)	0	$5/2^+$			67.0(47)	$E1$	0.181(45)		
2580.8(2)	$11/2^+$	535.95(28)	2045.5	$9/2^+$	0.330(339)	$>$19	18.1(28)	$E2+M1$		$<$0.41	$<$4690
		726.73(29)	1853.9	$11/2^+$			12.3(27)	$E2+M1$		$<$0.12	$<$734
		1122.88(41)	1457.3	$9/2^+$			33.8(58)	$E2+M1$		$<$0.084	$<$220
		2435.30(25)	145.44	$7/2^+$			35.9(65)	$E2$			$<$5.0
2583.0(5)	$7/2^-$	2437.22(77)	145.44	$7/2^+$	0.581(66)	35^{10}_{8}	33.5(4)	$E1$	$0.238^{0.073}_{0.056}$		
		2583.26(72)	0	$5/2^+$			66.5(4)	$E1$	$0.397^{0.120}_{0.091}$		
2601.2(5)	5/2,	2455.74(69)	145.44	$7/2^+$	0.358(104)	85^{53}_{29}	28.5(50)	$E1$	$0.082^{0.057}_{0.046}$		
	$7/2^-$	2601.30(84)	0	$5/2^+$			71.5(50)	$E1$	$0.172^{0.101}_{0.078}$		
2603.8(6)	5/2,	2458.73(66)	145.44	$7/2^+$	0.548(96)	40^{18}_{13}	20.0(24)	$E1$	$0.121^{0.073}_{0.052}$		
	$7/2^-$	2603.07(83)	0	$5/2^+$			80.0(24)	$E1$	$0.408^{0.209}_{0.139}$		
2607.1(8)	$1/2^+$	2607.06(76)	0	$5/2^+$	0.208(89)	180^{160}_{70}	100	$E2$			$0.88^{0.52}_{0.42}$
2611.7(5)	$9/2^+$	1318.59(46)	1292.4	$5/2^+$	0.537(42)	42^7_6	12.5(15)	$E2$			14.1(40)
		2612.42(72)	0	$5/2^+$			87.5(15)	$E2$			3.2(6)
2623.2(4)	(5/2,	1330.33(45)	1292.4	$5/2^+$	0.313(50)	104^{28}_{20}	16.8(24)	$E2+M1$		$\leqslant$0.0054	$\leqslant$10.1
	$7/2)^+$	2477.72(67)	145.44	$7/2^+$			40.0(24)	$E2+M1$		$\leqslant$0.0018	$\leqslant$1.01
		2623.81(75)	0	$5/2^+$			43.2(26)	$E2+M1$		$\leqslant$0.0017	$\leqslant$0.82

TABLE III. *(Continued.)*

E_i (keV)	J_i^π	E_γ (keV)	E_f (keV)	J_f^π	$F(\tau)$	τ (fs)	I_γ (%)	δ or πL	$B(E1)\downarrow$ (10^{-3} W.u.)	$B(M1)\downarrow$ (μ_N^2)	$B(E2)\downarrow$ (W.u.)
2646.5(5)	$9/2^+$	2500.60(69)	145.44	$7/2^+$	0.266(46)	130^{36}_{25}	45.6(26)	$E2+M1$		$\leqslant 0.0017$	$\leqslant 0.88$
		2646.91(75)	0	$5/2^+$			54.4(26)	$E2$			0.61(17)
2659.6(8)	$11/2^+$	2514.14(75)	145.44	$7/2^+$	0.086(84)	>225	100	$E2$			<0.83
2668.8(3)	$13/2^-$	1175.16(32)	1493.9	$11/2^+$	0.438(104)	61^{33}_{20}	13.3(20)	$E1$	$0.48^{0.31}_{0.24}$		
		1216.36(43)	1452.1	$7/2^+$			22.2(33)	$E3$			
		1551.26(42)	1117.2	$11/2^-$			64.5(32)	$0.176^{0.081}_{0.081}$		$0.0156^{0.0089}_{0.0066}$	$0.67^{1.41}_{0.57}$
								$10.1^{\infty}_{5.2}$		$0.0002^{0.0008}_{0.0002}$	$22.0^{12.1}_{9.3}$
2682.9(4)	(5/2,	870.93(41)	1812.4	$9/2^+$	0.127(60)	320^{320}_{120}	12.5(14)	$E2+M1$		$\leqslant 0.0057$	$\leqslant 24.9$
	$7/2)^+$	1246.08(54)	1436.0	$3/2^+$			6.7(12)	$E2+M1$		$\leqslant 0.0011$	$\leqslant 2.3$
		1556.27(41)	1126.5	$3/2^+$			49.1(19)	$E2+M1$		$\leqslant 0.0037$	$\leqslant 5.1$
		2537.5(11)	145.44	$7/2^+$			4.9(11)	$E2+M1$		$\leqslant 0.0002$	$\leqslant 0.05$
		2683.24(79)	0	$5/2^+$			26.8(21)	$E2+M1$		$\leqslant 0.0004$	$\leqslant 0.18$
2707.4(4)	$15/2^-$	1590.16(35)	1117.2	$11/2^-$	0.446(278)	60^{170}_{40}	100	$E2$			31^{66}_{23}
2709.8(4)	$3/2^+$	1411.33(32)	1298.4	$5/2^+$	0.165(117)	230^{670}_{115}	44.8(94)	$E2+M1$		$\leqslant 0.0085$	$\leqslant 14.0$
		1583.28(43)	1126.5	$3/2^+$			55.2(94)	$E2+M1$		$\leqslant 0.0072$	$\leqslant 9.6$
2718.4(4)	(9/2,	1197.53(36)	1520.9	$9/2^+$	0.037(132)	>230	68.0(25)	$E2+M1$		<0.0099	<22.8
	$11/2)^+$	1601.07(53)	1117.2	$11/2^-$			32.0(25)	$E1$	<0.12		
	(9/2,	1197.53(36)	1520.9	$9/2^+$	0.037(132)	>230	68.0(25)	$E1$	<0.63		
	$11/2)^-$	1601.07(53)	1117.2	$11/2^-$			32.0(25)	$E2+M1$		<0.0019	<2.5
2722.0(4)	$3/2^+$	1271.60(48)	1452.1	$7/2^+$	0.426(75)	64^{23}_{16}	15(10)	$E2$			$13.3^{13.3}_{12.4}$
		1422.39(58)	1298.4	$1/2^+$			10(10)	$E2+M1$		$\leqslant 0.0072$	$\leqslant 11.8$
		2576.04(88)	145.44	$7/2^+$			25(10)	$E2$			0.65(0.48)
		2721.48(82)	0	$5/2^+$			50(10)	$E2+M1$		$\leqslant 0.0034$	$\leqslant 1.52$
2731.5(4)	$9/2^+$	877.51(42)	1853.9	$11/2^+$	0.375(79)	79^{33}_{21}	3(3)	$E2+M1$		$\leqslant 0.0076$	$\leqslant 32.5$
		1278.65(45)	1452.1	$7/2^+$			22(10)	$E2+M1$		$\leqslant 0.014$	$\leqslant 27.8$
		2586.62(83)	145.44	$7/2^+$			50(10)	$0.036^{0.141}_{0.162}$		0.0021(12)	$<10^{-2}$
								$-7.0^{4.0}_{56.6}$		$<10^{-4}$	1.01(60)
		2732.12(84)	0	$5/2^+$			25(10)	$E2$			0.39(30)
2739.7(3)	$1/2^-$	1159.62(27)	1580.0	$5/2^-$	0.111(160)	>125	100	$E2$			<72
2777.5(5)	$9/2^+$	923.77(37)	1853.9	$11/2^+$	0.427(60)	64^{17}_{13}	17.0(23)	$E2+M1$		$\leqslant 0.027$	$\leqslant 103$
		2631.89(78)	145.44	$7/2^+$			83.0(23)	$-0.060^{0.091}_{0.098}$		0.0040(12)	$0.01^{0.05}_{0.01}$
								$-4.1^{1.2}_{2.9}$		$0.0002^{0.0003}_{0.0002}$	1.83(60)
	$9/2^-$	923.77(37)	1853.9	$11/2^+$	0.427(60)	64^{17}_{13}	17.0(23)	$E1$	1.21(47)		
		2631.89(78)	145.44	$7/2^+$			83.0(23)	$E1$	0.26(7)		
2781.8(6)	(5/2,	2637.37(81)	145.44	$7/2^+$	0.172(61)	222^{144}_{69}	65.9(34)	$E2+M1$		$\leqslant 0.0014$	$\leqslant 0.66$
	$7/2)^+$	781.84(89)	0	$5/2^+$			34.1(34)	$E2+M1$		$\leqslant 0.0006$	$\leqslant 0.27$
2782.3(8)	$13/2^+$	576.93(25)	2206.1	$11/2^+$	0.179(214)	>73	33(15)	$E2+M1$		<0.20	<1951
		1261.13(54)	1520.9	$9/2^+$			67(15)	$E2$			<66
2801.7(3)	$9/2^+$	1151.18(46)	1651.3	$9/2^+$	0.214(111)	170^{225}_{75}	37.2(33)	$E2+M1$		$\leqslant 0.015$	$\leqslant 38$
		2655.96(37)	145.44	$7/2^+$			33.6(32)	$E2+M1$		$\leqslant 0.0011$	$\leqslant 0.52$
		2801.76(27)	0	$5/2^+$			29.2(34)	$E2$			0.19(16)
2807.1(3)	$3/2^+$,	491.37(34)	2315.5	$5/2^+$	0.389(91)	74^{36}_{22}	7.5(75)	$E2+M1$		$\leqslant 0.12$	$\leqslant 1616$
		2661.96(42)	145.44	$7/2^+$			45.5(100)	$E2$			0.87(0.56)
		2807.13(22)	0	$5/2^+$			47.0(100)	$E2+M1$		$\leqslant 0.0026$	$\leqslant 1.13$
	$5/2^-$,	491.37(34)	2315.5	$5/2^+$	0.389(91)	74^{36}_{22}	7.5(75)	$E1$	$3.075^{3.351}_{3.057}$		
		2661.96(42)	145.44	$7/2^+$			45.5(100)	$E1$	$0.117^{0.075}_{0.064}$		
		2807.13(22)	0	$5/2^+$			47.0(100)	$E1$	$0.103^{0.066}_{0.056}$		
2811.0(3)	$1/2^+$	1201.08(45)	1608.2	$3/2^+$	0.085(211)	>110	45.7(66)	$E2+M1$		<0.016	<36
		2810.95(23)	0	$5/2^+$			54.3(66)	$E2$			<0.59
2813.9(3)	$1/2^-$	1233.07(36)	1580.0	$5/2^-$	579(185)	35^{37}_{20}	45.6(66)	$E2$			86^{127}_{57}

TABLE III. *(Continued.)*

E_i (keV)	J_i^π	E_γ (keV)	E_f (keV)	J_f^π	$F(\tau)$	τ (fs)	I_γ (%)	δ or πL	$B(E1)\downarrow$ (10^{-3} W.u.)	$B(M1)\downarrow$ (μ_N^2)	$B(E2)\downarrow$ (W.u.)
		1687.70(34)	1126.5	$3/2^+$			54.4(66)	$E1$	$1.16^{1.69}_{0.74}$		
2837.4(8)	(5/2,	2691.97(94)	145.44	$7/2^+$	0.588(115)	34^{19}_{13}	75.0(37)	$E1$	$0.41^{0.27}_{0.17}$		
	$7/2)^-$	2837.5(11)	0	$5/2^+$			25.0(37)	$E1$	$0.12^{0.09}_{0.06}$		
2839.6(3)	$9/2^-$	2694.17(39)	145.44	$7/2^+$	0.366(131)	81^{69}_{33}	100	$E1$	$0.23^{0.16}_{0.11}$		
2845.1(5)	$3/2^-$	1186.83(48)	1656.8	$1/2^+$	0.417(227)	65^{130}_{40}	25(15)	$E1$	$0.82^{1.67}_{1.03}$		
		1546.60(59)	1298.4	$5/2^+$			25(15)	$E1$	$0.37^{0.75}_{0.47}$		
		2846.2(11)	0	$5/2^+$			50(20)	$E1$	$0.12^{0.22}_{0.13}$		
2847.5(4)	$9/2^+$	1005.00(36)	1842.1	$7/2^+$	0.068(180)	>140	36.0(39)	$-0.20^{0.23}_{0.43}$		<0.016	<3.1
								$-2.5^{1.5}_{4.5}$		<0.0005	<51
		1353.97(54)	1493.9	$11/2^+$			18.0(28)	$E2+M1$		<0.0034	<6.1
		1389.89(57)	1457.3	$9/2^+$			14.9(29)	$E2+M1$		<0.0027	<4.6
		2702.8(12)	145.44	$7/2^+$			11.8(23)	$E2+M1$		<0.0003	<0.13
		2848.4(11)	0	$5/2^+$			19.3(64)	$E2$			<0.19
2863.1(8)	$^+$	1570.93(56)	1292.4	$5/2^+$	0.363(343)	80^{2170}_{60}	66.6(200)	$E2+M1$		$\leqslant$0.053	$\leqslant$70
		2716.8(15)	145.44	$7/2^+$			33.3(200)	$E2+M1$		$\leqslant$0.0055	$\leqslant$2.4
	$^-$	1570.93(56)	1292.4	$5/2^+$	0.363(343)	80^{2170}_{60}	66.6(200)	$E1$	$0.75^{2.57}_{0.75}$		
		2716.8(15)	145.44	$7/2^+$			33.3(200)	$E1$	$0.073^{0.270}_{0.073}$		
2881.7(5)	7/2,	1028.04(46)	1853.9	$11/2^+$	0.150(222)	>80	23.7(108)	$E2+M1$		<0.023	<71
	$9/2^+$	1424.45(78)	1457.3	$9/2^+$			25.8(129)	$E2+M1$		<0.0096	<15.8
		1428.46(62)	1452.1	$7/2^+$			21.5(53)	$E2+M1$		<0.0066	<10.7
		2737.0(16)	145.44	$7/2^+$			7.5(42)	$E2+M1$		<0.0004	<0.19
		2882.3(11)	0	$5/2^+$			21.5(43)	$E2+M1$		<0.0001	<0.31
2887.5(4)	(9/2,	1075.23(53)	1812.4	$9/2^+$	0.222(368)	>35	23.6(56)	$E2+M1$		<0.041	<116
	$11/2)^+$	1366.96(38)	1520.9	$9/2^+$			28.1(56)	$E2+M1$		<0.023	<41
		1392.82(52)	1493.9	$11/2^+$			22.5(56)	$E2+M1$		<0.018	<31
		1769.60(56)	1117.2	$11/2^-$			16.9(101)	$E1$	0.33(0.20)		
		2742.5(17)	145.44	$7/2^+$			9.0(34)	$E2+M1$		<0.0011	<0.46
	$9/2^-$	1075.23(53)	1812.4	$9/2^+$	0.222(368)	>35	23.6(56)	$E1$	2.07(49)		
		1366.96(38)	1520.9	$9/2^+$			28.1(56)	$E1$	1.20(24)		
		1392.82(52)	1493.9	$11/2^+$			22.5(56)	$E1$	0.91(23)		
		1769.60(56)	1117.2	$11/2^-$			16.9(101)	$E2+M1$		<0.0084	<8.9
		2742.5(17)	145.44	$7/2^+$			9.0(34)	$E1$	0.048(18)		
2897.1(8)	$11/2^+$	1438.97(78)	1457.3	$9/2^+$			29.2(104)				
		2752.04(95)	145.441	$7/2^+$			70.8(104)				
2929.2(5)	(5/2,	1635.97(48)	1292.4	$5/2^+$	0.288(165)	115^{205}_{60}	48.2(54)	$E2+M1$		$\leqslant$0.012	$\leqslant$14.4
	$7/2)^+$	2785.2(11)	145.44	$7/2^+$			41.1(54)	$E2+M1$		$\leqslant$0.002	$\leqslant$0.87
		2930.3(12)	0	$5/2^+$			10.7(27)	$E2+M1$		$\leqslant$0.0005	$\leqslant$0.18
2941.4(8)		1484.2(10)	1457.3	$9/2^+$			21.1(132)				
		1488.55(76)	1452.1	$7/2^+$			21.1(132)				
		2796.4(14)	145.44	$7/2^+$			26.3(79)				
		2941.7(14)	0	$5/2^+$			31.6(79)				
2950.3(9)	$1/2^+$	1514.40(64)	1436.0	$3/2^+$			67(15)				
		2950.1(17)	0	$5/2^+$			33(15)				
2983.0(3)	(5/2,	2839.0(7)	145.4	$7/2^+$			18(11)				
	$7/2)^-$	2983.04(46)	0	$5/2^+$			82(11)				
3000.7(3)	$11/2^+$	955.95(42)	2045.5	$9/2^+$			30(11)				
		1479.49(51)	1520.9	$9/2^+$			20(11)				
		2855.20(26)	145.44	$7/2^+$			50(9)				
3016.0(8)	$5/2^-$	940.96(47)	2075.4	$5/2, 7/2^+$			32.8(78)				
		1887.9(13)	1126.5	$3/2^+$			17.4(63)				
		2871.0(19)	145.44	$7/2^+$			12.5(47)				
		3015.9(15)	0	$5/2^+$			34.4(63)				
3034.1(8)	$1/2^+$	1734.94(69)	1298.4	$5/2^+$			60(20)				

TABLE III. *(Continued.)*

E_i (keV)	J_i^π	E_γ (keV)	E_f (keV)	J_f^π	$F(\tau)$	τ (fs)	I_γ (%)	δ or πL	$B(E1)\downarrow$ (10^{-3} W.u.)	$B(M1)\downarrow$ (μ_N^2)	$B(E2)\downarrow$ (W.u.)
		1742.49(76)	1292.4	$1/2^+$			40(20)				
3045.6(8)	$11/2^+$,	1524.57(66)	1520.9	$9/2^+$			54(10)				
	9/2	2900.2(12)	145.44	$7/2^+$			46(10)				
3064.2(7)	$9/2^-$	960.45(59)	2104.9	$5/2^-$			32(21)				
		1209.90(55)	1853.9	$11/2^+$			30(12)				
		2918.4(12)	145.44	$7/2^+$			38(8)				
3075.3(14)	$3/2^+$	1623.1(11)	1452.1	$7/2^+$			52(20)				
		3075.4(15)	0	$5/2^+$			48(20)				
3079.8(10)		1094.0(5)	1985.8	$13/2^+$			53(23)				
		2934.1(17)	145.44	$7/2^+$			47(23)				
3083.4(14)		3083.4(14)	0	$5/2^+$			100				
3114.7(12)		2969.2(19)	145.44	$7/2^+$			67(17)				
		3114.8(15)	0	$5/2^+$			33(17)				
3129.5(7)		764.56(50)	2362.8	$5/2^-$			21(13)				
		1838.08(66)	1292.4	$1/2^+$			39.4(95)				
		3128.7(16)	0	$5/2^+$			39.6(95)				
3156.0(8)		1180.31(73)	1975.2	$3/2^+$			28.6(95)				
		1497.7(14)	1656.8	$1/2^+$			14.3(95)				
		1574.7(13)	1580.0	$5/2^-$			23.8(119)				
		3011.2(12)	145.44	$7/2^+$			33.3(71)				

[a]Multipole-mixing ratio taken from Refs. [36,37].

[b]The 649 keV γ ray was not resolved; see text for a discussion.

[c]The 669 keV γ ray could not be resolved from a background transition but is included by using the intensity value given in Ref. [18], relative to the 604 keV transition.

given as upper limits. If just upper limits were obtained, the upper uncertainties are contained in the values, otherwise both errors are listed.

Aspects that caused major problems during the analysis or shed new light on parts of the level scheme found in the data compilations [18,36] are now presented. The 649 keV peak proved, at neutron energies over 2.3 MeV, to contain γ rays from the states at 1767 and 2228 keV, respectively.

The 882.6 keV γ ray was previously assigned as deexciting the $9/2^-$ level observed in this experiment at 2000.4 keV. The excitation functions as shown in Fig. 3 indicate that this γ ray originates from a second level (spin $15/2^-$) at 1999.8 keV.

For the 2004.1 keV level, a ground-state transition is reported in Refs. [18,36]. In this experiment, only a background peak was observed at this energy. The angular distribution observed for the strong 1858 keV transition from the state at 2004 keV points toward a spin assignment of $J = 11/2$. This spin would require a possible ground-state transition to have an $M3$ multipolarity if the state has positive parity and an $E3$ multipolarity for a negative-parity state. It appears that this transition does not exist. Furthermore, no evidence was found for the γ rays from the previously assigned states at 1455, 1910, and 1913.5 keV.

From the shape of the excitation function, the 465 keV transition was totally attributed to the 1986 keV level, despite the alternative placement to the 2045 keV level in the data compilation [18,36]. The 524.1 keV transition attributed to this level was assigned to the 2105 keV level, based upon the excitation function.

Neither of the two transitions (272.7 and 301.4 keV) attributed to the 2069.7 keV level could be resolved from the obscuring peaks of the 272.3 (2126.2 $\rightarrow$ 1853.9 keV) and the 301.9 keV (1796.1 $\rightarrow$ 1493.9 keV) transitions.

Previously, states were identified at 2075.5 and 2075.7 keV. The excitation functions indicate that the four transitions assigned to these two states stem, in fact, from a single state at 2075.4 keV.

A comparison of the shape of the excitation function of the 987.8 keV γ ray depopulating the 2105.0 keV state with those observed for the 1959.4 and 2105 keV γ rays led to the assignment of a second state at 2104.9 keV.

For the state at 2126 keV, the 669 keV decay γ ray could not be resolved from a background peak. For this analysis, the branching ratio with respect to the 604 keV transition, given in the literature as 602.4 keV, was used. The deviation from the energy given in the literature (2124 keV) is caused by the deviation of the 604.9 keV γ ray observed in this work with respect to the literature value of 602.4 keV. However, it is confusing that a 1981 keV γ ray was also observed in NRF experiments [25]. The $11/2^+$ spin assignment to this level results in a spin difference of $\Delta J = 3$ to the ground state, which means that it is impossible to excite this state in NRF experiments directly. Also, no ground-state transition was observed in this experiment. This absence can be seen as proof of unobserved feeding from higher lying levels in the NRF experiments.

The 2354.8 keV γ ray was previously assigned as the ground-state transition of a state at this energy, but the

excitation function shows unambiguously that it is the decay of the level at 2500.2 keV to the first excited state. Furthermore, the shape of its excitation function indicates that the peak at 2500.6 keV is dominated by the decay from a state at 2646.5 keV. It was not possible to resolve both transitions, and the whole peak was attributed to the 2646.5 → 145.4 keV transition.

In Ref. [25], a state was placed at 2602 keV with a decay branch (2457 keV) to the first excited state. The spectra obtained in this experiment showed the peaks at both energies to be very wide, even for Doppler-broadened peaks. Accordingly, a doublet was fitted for both. However, some uncertainty remains and, instead of the states at 2601.2 and 2603.8 keV assigned in this work, there might be only one state at 2602 keV, as pointed out in the NRF measurement.

The excitation functions showed that the states assigned in NRF at 2586 and 2786 keV are decays to the first excited state at 145 keV from states at 2731.5 and 2929.2 keV, respectively. For both states, these decays are a factor of 3 to 4 stronger than the ground-state decay, so the ground-state decays were simply below the sensitivity limit in the NRF measurement.

The 2982 keV γ ray, which was seen in the NRF experiments to decay to the first excited state, is in fact the ground-state transition of a state at 2983.0 keV. The assignment of the 2839 keV γ ray as a decay to the first excited state, and not as a ground-state decay to the level observed at this energy, was chosen because of the excitation function. In general, the construction of the level scheme above approximately 2.7 MeV faces the difficulty that the population of the levels in this region is reduced. Furthermore, the excitation functions consist only of a small number of points, thus it is often impossible to draw any definite conclusions about the thresholds.

As mentioned previously, it was uncertain if the $E1$ strength in the NRF measurements from the $[[2^+ \otimes 3^-] \otimes particle]$ states was correct, because transitions were either hidden in the background or simply wrongly assigned. A comparison of the NRF study and the study presented in this paper revealed that several γ-ray transitions assigned in the NRF data to be ground-state transitions of excited states at the respective energy, were not observed in the INS at all. Except for the 2954 keV γ ray, it is likely that these transitions stem from states with excitation energies higher than the maximum neutron energy used in these $(n, n'\gamma)$ studies. The transitions are given together with their possible new assignments in the level scheme in Table IV. For possible combinations ($E_i - E_f \leqslant 2$ keV), the restriction has been made that the spin of the final state must be accessible with two $E2$ transitions from the ground state. However, most of the transitions newly assigned in Table IV are extremely weak, so even when they stem from the quadrupole-octupole particle coupled states, they do not carry enough strength to account for the greater $E1$ strengths observed for the core nuclei.

TABLE IV. γ rays observed in NRF experiments [25] but not in the present inelastic neutron scattering studies. Their possible placements in the level scheme are given (see discussion in the text) together with their energies.

E_γ (keV)	E_i (keV)	E_f (keV)
1559	3016	1457
	3346	1786
	3370	1812
	3659	2101
1816	3338	1521
	3659	1842
	3791	1975
1849	3370	1521
	3427	1580
2270	3706	1435
	3791	1521
	3879	1608
2296	3791	1494
2954	–	–

IV. DISCUSSION

In this section, the observed states are discussed in the framework outlined in the Introduction. As previously mentioned, detailed knowledge of the decay scheme, spins, parities, and transition multipolarities is crucial for an interpretation.

A. Positive-parity states

As pointed out earlier, states with a dominant single-particle component in their wave functions can be identified from particle transfer reactions. For the ground state and the first two exited states, a nearly pure one-particle wave function can be assumed due to the large energies (>1 MeV) to the next states with identical spins. For the two proposed $1/2^+$ states, the 1657 keV state shows an expected weak $E2$ transition to the ground state, while the state at 1299 keV exhibits a large, collective $E2$ transition to the ground state. This indicates that there is little mixing between these states; otherwise, the $E2$ strength would be distributed over both states. It can therefore be concluded that the state at 1657 keV has an almost pure $|\Psi\rangle = |3s_{1/2}\rangle$ wave function, and the state at 1299 keV is of nearly pure $[2_1^+ \otimes d_{5/2}]_{1/2}$ nature. The $3/2^+$ state at 1608 keV has a transition strength much too strong for pure $E2$ multipolarity. This result, in agreement with the particle transfer reactions, displays the expected strong $|d_{3/2}\rangle \rightarrow |d_{5/2}\rangle M1$ spin-flip nature of this transition.

All other states observed below 1.7 MeV show strong transitions either to the ground state or to the first excited state. These states can be identified as belonging to the $[2^+ \otimes p_j]$ ($p_j = d_{5/2}, g_{7/2}$) particle-core coupled multiplets expected in the energy range near the first 2^+ excitation in the core nuclei. Additionally, the state at 1786 keV is seen to be a member of these multiplets. States with a dominant single-particle component and those of $2^+ \otimes particle$ origin are shown in Fig. 7. The $1/2^+$ level at 1298 keV is a nearly pure $[2^+ \otimes d_{5/2}]$ state. Further, the $11/2^+$ state at 1494 keV is of pure $[2^+ \otimes g_{7/2}]$ character. The $[2^+ \otimes p_j]_{5/2}$ states show the expected strong mixing, as indicated by the almost equal

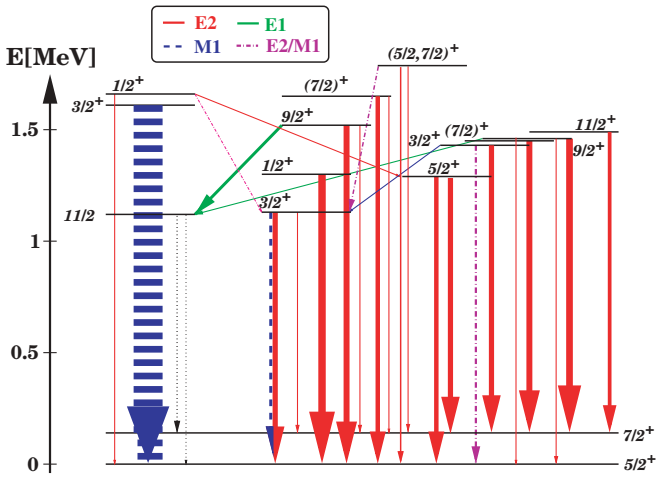

FIG. 7. (Color online) Partial level scheme of ^{141}Pr showing the states with either a dominant $\alpha|p_i\rangle$ single-particle component in the wave function plotted to the left or states with a major $\beta_j|2^+ \otimes p_j\rangle (p_j = d_{5/2}, g_{7/2})$ component, belonging to the $[2^+ \otimes p_j]$ multiplets. Lines depict an almost pure $E2$, an $M1$, an $E1$, and a mixed $E2$/M1 transition (see legend). The thickness of the arrow is proportional to the observed transition strength. For a detailed discussion, see the text.

decay strength to either of the two single-particle states and the considerably large energy difference between them. The $(5/2, 7/2)^+$ state at 1786 keV shows a transition to the state at 1127 keV, which gives evidence for a further component admixed into its wave function. Astonishingly, the 7/2 and 9/2 states decay strongly to one of the single-particle states and very weakly to the other. This decay behavior implies that these states mix only weakly.

The two $[2^+ \otimes p_j]_{3/2}$ states show enhanced ground state transitions compared to the other members of the multiplets. It is likely that both states have an admixture of the $d_{3/2}$ subshell giving rise to a $d_{3/2} \rightarrow d_{5/2}M1$ spin-flip component in their ground-state transitions. Unfortunately, the spin is lower than the ground-state spin, thus the multipole-mixing ratios for these transitions cannot be determined in $(n, n'\gamma)$ experiments. In Ref. [36], a multipole-mixing ratio $\delta = 0.47(6)$, measured in Coulomb excitation [37], for the ground-state transition of the 1127 keV state was given. The Coulomb excitation data show discrepancies when compared with other available data sets; thus for this analysis only this single value will be used, because previous unpublished NRF data [8] confirm this value of δ.

Using the experimentally observed transition strengths, we can quantify the empirical approach used so far. Neglecting the single-particle components and assuming that the wave functions of these levels consist exclusively of quadrupole phonon-particle coupled components, we can make the ansatz of a simple two-state mixing:

$$\begin{aligned} |\Psi_I\rangle_J &= \beta_1|2_1^+ \otimes d_{5/2}\rangle_J + \beta_2|2_1^+ \otimes g_{7/2}\rangle_J, \\ |\Psi_{II}\rangle_J &= \beta_2|2_1^+ \otimes d_{5/2}\rangle_J - \beta_1|2_1^+ \otimes g_{7/2}\rangle_J. \end{aligned} \tag{6}$$

Furthermore, we assume that particle-core coupled states only decay to the particle state when the particle is identical $|\langle p_i|\hat{O}|[Q^+ \otimes p_j]_J\rangle|^2 \propto B(\Pi L)\delta_{ij}$. Together with the normalization condition $1 = \alpha^2 + \beta^2$ one can derive the mixing coefficients α and β from the ratios $R_i (i = I, II)$:

$$R_i = \frac{B(E2, |\Psi_i\rangle_J \rightarrow |d_{5/2}\rangle)}{B(E2, |\Psi_i\rangle_J \rightarrow |g_{7/2}\rangle)}. \tag{7}$$

Using the crude approximation that the transition strength is only given by the core parts of the coupled wave functions so that $(|\langle d_{5/2}|\hat{E2}|[2^+ \otimes d_{5/2}\rangle|^2 \approx |\langle g_{7/2}|\hat{E2}|[2^+ \otimes g_{7/2}\rangle|^2)$, the mixing amplitudes are calculated as

$$\begin{aligned} \beta_1 &= \sqrt{\frac{R_I}{1+R_I}} = \sqrt{\frac{1}{1+R_{II}}}, \\ \beta_2 &= \sqrt{\frac{1}{1+R_I}} = \sqrt{\frac{R_{II}}{1+R_{II}}}. \end{aligned} \tag{8}$$

The interaction strength between the states of a given angular momentum J of the two multiplets can be calculated from

$$V_{mix} = \beta_1\beta_2(E_I - E_{II}), \tag{9}$$

where the energies $E_i (i = \mathrm{I}, \mathrm{II})$ are the experimentally observed energies of the mixed states.

The results for the mixing amplitudes and the resulting mixing matrix elements V_{mix} (given in Table V) confirm the low degree of mixing for the $7/2^+$ and $9/2^+$ states. For the $[2_1^+ \otimes d_{5/2}]_{3/2}$ fragments, the $M1$ spin-flip contamination obscures the expected $E2$ parts of the transitions. Accordingly, the β_i $(i = 1, 2)$ coefficients can only be seen as an approximation to the mixing of the particle-core coupled states. If the other two multipole-mixing ratios $(1608 \rightarrow 0, 1436 \rightarrow 0)$ were known, a similar procedure to that proposed in Ref. [38] could have been applied for a total resolution of this three-state mixing by separating the $M1$ parts in a first step.

The $5/2^+$ states show a considerable degree of mixing, in contrast to the other states of both multiplets. This is manifest in the nearly equal decay strengths as well as in the relatively large energy gap between the two states. The higher lying $5/2^+$ state at 1786 keV decays to the state at 1127 keV, indicating a further component in this wave function. From the comparable decay strength, it is most likely a $[0_2^+ \otimes d_{5/2}]$ component decaying with a collective $E2$ transition to the $[2^+ \otimes d_{5/2}]$ component of the 1127 keV state. Nevertheless, it can be stated that the multiplets in general do not show the expected strong mixing.

A calculation of the unperturbed energies of the pure $E_{[2^+ \otimes p_j]}$ states,

$$\begin{aligned} E_{[2^+ \otimes d_{5/2}]} &= \frac{\beta_1 E_I \pm \beta_2 V_{mix}}{\beta_1} \\ &= \frac{\beta_2 E_{II} \pm \beta_1 V_{mix}}{\beta_2}. \\ E_{[2^+ \otimes g_{7/2}]} &= \frac{\beta_2 E_I \pm \beta_1 V_{mix}}{\beta_2} \\ &= \frac{\beta_1 E_{II} \pm \beta_2 V_{mix}}{\beta_1}. \end{aligned} \tag{10}$$

TABLE V. Calculated mixing coefficients β_1, β_2 for the mixed states with a major $\sum_i [2_1^+ \otimes p_i]_J (p_i = d_{5/2}, g_{7/2})$ component from the data from Table III and Eqs. (6)–(8). A discussion is given in the text.

J^π	$E_{\rm I}$ (keV)	$E_{\rm II}$ (keV)	$R_{\rm I}$	$R_{\rm II}$	$\beta_1(R_{\rm I})$	$\beta_2(R_{\rm I})$	$V_{\rm mix\,I}$ (keV)	$\beta_1(R_{\rm II})$	$\beta_2(R_{\rm II})$	$V_{\rm mix\,II}$ (keV)
$3/2^+$[a]	1127	1436	3.3(6)	0.51(30)	0.88(3)	0.48(6)	126(19)	0.81(23)	0.58(16)	146(81)
$5/2^+$	1292	1786	1.4(7)	0.82(43)	0.76(17)	0.65(19)	244(126)	0.74(19)	0.67(18)	246(129)
$7/2^+$	1651	1452	7.4(18)	0.13(8)	0.94(3)	0.35(8)	64(16)	0.94(18)	0.34(7)	64(25)
$9/2^+$	1520	1457	6.3(24)	0.21(10)	0.93(5)	0.37(12)	22(8)	0.91(16)	0.42(8)	24(9)

[a]Wave functions contain an additional $\alpha|d_{3/2}\rangle$ component.

resulted in the values presented in Table VI and shown in Fig. 8. As some states of the $[2^+ \otimes d_{5/2}]_J$ multiplet are higher lying and some are lower lying than the adjacent J state of the $[2^+ \otimes g_{7/2}]_J$ multiplet, the signs of the terms containing the mixing interaction $V_{\rm mix}$ vary. The use of the different data sets based on the experimentally observed E_i and $R_i (i = {\rm I}, {\rm II})$ results in slightly different energies for the unmixed states. For Table VI, the average was taken. For the $3/2^+$ states, only data set II for the decays to the $g_{7/2}$ subshell at 145 keV was considered. For these states, the comparably low excitation energies display the unresolved mixing with the $d_{3/2}$ subshell.

The pure $[2^+ \otimes d_{5/2}]_J$ states exhibit a larger energy splitting than the pure $[2^+ \otimes g_{7/2}]_J$ states. The centers of gravity are nearly equal for both multiplets ($\langle E_{[2^+\otimes d_{5/2}]}\rangle = 1482$, $\langle E_{[2^+\otimes g_{7/2}]}\rangle = 1468$ keV). If the obscured $3/2^+$ states are neglected, the states for particle-hole coupling with the hole in the $g_{7/2}$ subshell are observed at lower energies than those for the particle coupled in the $d_{5/2}$ subshell ($\langle E_{[2^+\otimes d_{5/2}]}\rangle = 1536$, $\langle E_{[2^+\otimes g_{7/2}]}\rangle = 1489$ keV). Both results can be seen as evidence of different particle-core couplings in the sense that the core is different. In a pure particle picture, where the pairing force and the smoothing out of the Fermi level due to the influence of the pairing force are neglected, the best choice of a core nucleus for the single particle in the $d_{5/2}$ ground state is ^{140}Ce with its fully filled $g_{7/2}$ subshell, while by exciting a second particle to the $d_{5/2}$ subshell and creating the hole in the $g_{7/2}$ subshell, the shell model configuration of ^{142}Nd is created. Therefore, it is reasonable that the multiplets are observed at nearly the same energies, and the lower lying center of gravity for the $g_{7/2}$ multiplet is explained by considering the slightly lower excitation energy of the first quadrupole excitation in ^{142}Nd compared to ^{140}Ce. A second reason for the lowering observed for this multiplet is the stronger mixing with higher lying particle-core coupled states. The angular momenta of the next excitations in the core nuclei are 0^+, 4^+, and 6^+, resulting in a higher number of particle-core coupled states with a comparably high angular momentum. The states of the $[2^+ \otimes g_{7/2}]$ multiplet have, compared to the states $[2^+ \otimes d_{5/2}]$ multiplet, an average of one unit higher angular momentum and find more states with the same angular momentum with which to.

The different degrees of spreading of the level energies of one multiplet can be explained by the average deformed field the coupled particle experiences while orbiting the dynamical deformed core. The particle in the $d_{5/2}$ subshell orbits outside the ^{140}Ce core, while the hole in the $g_{7/2}$ subshell orbits within this subshell and is not affected by the field created by the two valence neutrons in the $d_{5/2}$ subshell of the ^{142}Nd core. In this simple picture, a smaller interaction of the particle and the core can be expected.

In a conservative approach, taking the lower limit of the 1127 keV state as its lifetime and using the multipole-mixing

TABLE VI. Experimentally observed energies E_i $(i = {\rm I}, {\rm II})$ and the energies of the pure $[2^+ \otimes d_{5/2}]_J$ and $[2^+ \otimes g_{7/2}]_J$ states, respectively. The values of the pure states are the averages of the two different R_i data sets in Table V.

J	$E_{\rm I}$ (keV)	$E_{\rm II}$ (keV)	$E_{[2^+\otimes d_{5/2}]}$ (keV)	$E_{[2^+\otimes g_{7/2}]}$ (keV)
$3/2^+$[a]	1127	1435	1199	1342
$5/2^+$	1786	1292	1572	1508
$7/2^+$	1651	1452	1627	1475
$9/2^+$	1520	1457	1512	1468

[a]Wave functions contain an additional $\alpha|d_{3/2}\rangle$ component.

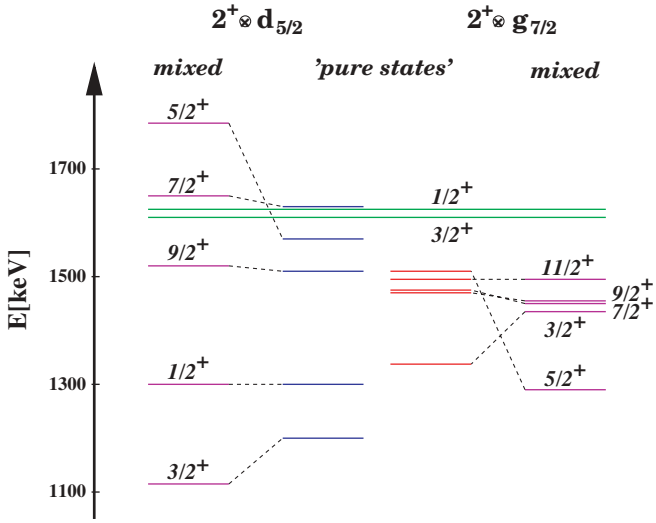

FIG. 8. (Color online) Level sequence of the $[2^+ \otimes p_j]$ particle-core coupled multiplets. The experimentally observed sequences (magenta) are compared to the results obtained after correcting for the two-state mixing between the two respective multiplets (red and blue). Not included in the corrections is the influence of the states with a dominant single-particle component in their wave functions (green).

TABLE VII. Global properties of the $[2^+ \otimes p_i]$ couplings in ^{141}Pr in comparison to the core nuclei ^{140}Ce and ^{142}Nd. Version I takes only the states with a major $[2^+ \otimes p_i]$ component into account, while version II includes the respective transitions of states up to 2.4 MeV. A detailed discussion is given in the text.

Nucleus	p	E_{2^+} or $\langle E \rangle$ (keV)	$B(E2, 0^+ \to 2^+)$ or $\sum_J B(E2, p \to [2^+ \otimes p]_J)$ (W.u.)	$\sum B(E2) \uparrow_{\text{odd}} / B(E2) \uparrow_{^{140}\text{Ce}}$ (%)	$\sum B(E2) \uparrow_{\text{odd}} / B(E2) \uparrow_{^{142}\text{Nd}}$ (%)
^{140}Ce		1596	69.0(15)1[a]		
^{141}Pr	$d_{5/2}$ I	1462	50.8(37)	73.6	84.5
	II	1509	54.8(38)	78.8	91.1
	$g_{7/2}$ I	1448	45.6(61)	66.8	75.8
	II	1534	53.2(63)	77.1	88.4
^{142}Nd		1576	60.15(22)[a]		

[a]Data taken from Ref. [18].

ratios which lead to higher $B(E2)$ values, the total decaying $E2$ strength of all the $\sum_j [2^+ \otimes d_{5/2}] \to d_{5/2}$ transitions is calculated to be $\sum_J B(E2) \downarrow = 50.5(53)$ W.u. The $E2$ excitation strength is connected to the deexcitation strength by $B(E2) \uparrow = \frac{2J_u+1}{2J_l+1} B(E2) \downarrow$, where the subscript l denotes the lower lying and u the higher lying level. The statistical factor $\frac{2J_u+1}{2J_l+1}$ normalizes the transition strength to the number of m substates involved. The total $E2$ excitation strength calculated as $\sum_J B(E2) \uparrow = 50.1(37)$ W.u. equals the deexcitation $E2$ strength. For the $E2$ strength of the $[2^+ \otimes d_{5/2}]_{3/2}$ state at 1127 keV, we assumed that the same ratio of $E2$ strength was transferred from the ground-state decay of this state to the ground-state decay of the $d_{3/2}$ level at 1608 keV as $M1$ strength was transferred from this decay to the 1127 $\to$ ground-state decay. Therefore, we get an additional $B(E2) \downarrow = 1.19(14)$ W.u. Furthermore, it cannot be excluded that the ground-state $E2$ decay strength of states with excitation energies above that of the $[2^+ \otimes p_j]$ states is generated by a mixing of $[2^+ \otimes d_{5/2}]$ configurations into the wave functions of these states. The strength of the ground-state decays of all positive-parity states not considered so far [$\sum B(E2) \downarrow = 4.6(6)$ W.u., $\sum B(E2) \uparrow = 4.0(7)$ W.u.] up to 2.4 MeV was added to allow a comparison of the summed $E2$ strength observed for the entire $[2^+ \otimes d_{5/2}]$ multiplet with the strength of the quadrupole excitations of the respective core nucleus. Thus the total $E2$ strength sums to $\sum B(E2, d_{5/2} \to [2^+ \otimes d_{5/2}]) = 54.8(38)$ W.u. The total $E2$ deexcitation strength $[2^+ \otimes g_{7/2}]$ to the level at 145 keV associated with the $g_{7/2}$ subshell is $B(E2) \downarrow = 47.3(55)$ W.u. For this multiplet, the sum rule of equal down- and up-going strength is fulfilled by an up-going value of $B(E2) \uparrow = 45.6(61)$ W.u. An additional amount, $B(E2) \uparrow = 7.6(17)$ W.u., is gained by assuming that the transitions to the 145 keV level from the positive-parity states up to 2.4 MeV stem from $[2^+ \otimes g_{5/2}]$ admixtures in their wave functions, thus the total amount of $E2$ strength is calculated as $\sum B(E2, g_{7/2} \to [2^+ \otimes g_{7/2}]) = 53.2(63)$ W.u. Here, the higher degree of mixing of the $[2^+ \otimes g_{7/2}]$ multiplet manifests itself in the larger amount of additional $E2$ strength found in the states between 1.8 and 2.4 MeV.

Even with this conservative approach for the summed $E2$ strength, both multiplets possess less strength than expected compared to the $0^+ \to 2^+$ transitions in the neighboring even-even core nuclei. This observation can be seen as a final confirmation of the nuclear structure effect suggested by the paucity of $E1$ strength observed for the $[[2^+ \otimes 3^-] \otimes p_i]$ states in NRF experiments [25]. While there was only 60% of the $E1$ strength compared to that measured in the core nuclei, the $[2^+ \otimes p_i]$ states show approximately 80% (^{140}Ce) and 90% (^{142}Nd) of the $E2$ strength observed in the core nuclei. Together with the reduced mixing of the $J = 7/2$ and $J = 9/2$ doublets, the reduced strength for both multiplets can be seen as strong evidence for the Pauli blocking mechanism proposed in Ref. [25]. As shown by the QPM calculations mentioned in the Introduction, the first 2^+ state in ^{140}Ce consists mainly of the $[g_{7/2}]^2$, $[d_{5/2}]^2$, and $[g_{7/2}, d_{5/2}]^2$ components. With the proton in the $d_{5/2}$ or $g_{7/2}$ subshell coupled to this core excitation, the configuration space for the proton pairs creating the core excitation in the respective subshell becomes truncated. Thus, when the particle p_i is coupled, the components $[p_i]^2$ and $[p_i, p_j]$ are affected, while the $[p_j]^2$ component remains undisturbed. Consequently, the core wave functions differ after coupling the particle in the two respective subshells. Therefore, the low degree of mixing observed in this experiment can be explained by

$$|\Psi_{\text{core}}(2^+ \otimes d_{5/2})\rangle \neq |\Psi_{\text{core}}(2^+ \otimes g_{7/2})\rangle. \tag{11}$$

This effect might even be stronger if one considers that the different couplings start with different core wave functions. For ^{142}Nd, the $[d_{5/2}]^2$ component increases, and the $[g_{7/2}]^2$ component decreases compared to the components for ^{140}Ce [19], as discussed in the Introduction. Furthermore, from QPM calculations for ^{144}Sm [20], the 2_1^+ RPA phonons show an increase of other components, e.g., $[h_{11/2}]^2$ or $[d_{5/2}, s_{1/2}]$. The observed lack of $E2$ strength indicates a truncation of the already very limited configuration space in the presence of the unpaired proton, leading to a loss of collectivity compared to the undisturbed core systems. The reduced $E2$ strengths can be explained by the blocking of different components in the core wave function and the resulting different core wave functions themselves. The relative difference of the blocking is proportional to the product of the branching ratios defined in Eq. (7):

$$\frac{\langle d_{5/2}|\hat{E2}|\Psi\rangle}{\langle g_{7/2}|\hat{E2}|\Psi\rangle} = \sqrt[4]{R_{\text{I}} R_{\text{II}}}. \tag{12}$$

Thus, in the calculation of the mixing amplitudes, this different blocking should have been taken into account. Nevertheless, other than for the $3/2^+$ states, these corrections are smaller than 10%, which is still below the experimental errors, so neglecting them can be justified. The reduction of the strength is proportional to the blocking the wave function experiences via the transition matrix element $\langle p_j|\hat{E2}|2^+ \otimes p_j\rangle$. We find that, relative to the ^{140}Ce core, approximately 10% of the core wave function is blocked and only approximately 5% in the case of ^{142}Nd. As the pairing force links the pairs in the m and $-m$ substates, we can assume that the proton in the $d_{5/2}$ subshell blocks one-third, and the hole in the $g_{7/2}$ subshell one-quarter of the respective subshell from contributing to the core excitation. In other words, by considering the Pauli exclusion principle, the unpaired proton probes the microscopic structure of the collective core excitations. The experimental results show that the $d_{5/2}$ subshell contributes approximately 30% to the first 2^+ excitation in ^{140}Ce, and the $g_{7/2}$ subshell nearly 20% to the 2^+_1 state in ^{142}Nd.

An interpretation of the positive-parity states above the previously discussed single-particle and $[2^+ \otimes p_i]$ dominated states gets more complicated thanks to the higher density of states (see Fig. 5), and enhanced mixing can be expected. In the particle-core coupling picture, these states originate from the coupling of the particle in the $d_{5/2}$ subshell or the hole in the $g_{7/2}$ subshell to the relatively collective 0^+ state, or the 4^+_1 and 6^+_1 states based mainly on the $[g_{7/2}]^2$ structure [20]. In fact, in the region above the $13/2^+$ state at 1767 keV, a number of states with comparably high spins are found. Along with an $E1$ decay to the $h_{11/2}$ state at 1117 keV, the 1767 keV state decays to the $[2^+ \otimes g_{7/2}]_{11/2}$ state at 1494 keV, indicating a $[4^+_1 \otimes g_{7/2}]$ component in its wave function. The same arguments can be used for the $15/2^+$ level at 1796 keV. The $13/2^+$ level at 1986 keV shows a decay to the 1767 keV level that corresponds to the $[g_{7/2}]^2_{6^+} \rightarrow [g_{7/2}]^2_{4^+}$ decay in the core nuclei. This state also decays to the 1521 keV level, the wave function of which is dominated by a $[2^+ \otimes d_{5/2}]$ component indicating a second $[[g_{7/2}]^2_{4^+} \otimes d_{5/2}]$ component in its wave function. A further candidate for a $[6^+ \otimes g_{7/2}]$ state is the $15/2^+$ state at 2108 keV.

Apart from these examples, a detailed interpretation of the observed states becomes nearly impossible because of the mixing effects and the experimental uncertainties in the spins assignments, the unknown multipole-mixing ratios, and the overall uncertainty of the level scheme. While, in the particle-core coupling picture the predicted number of four ($[0^+_2 \otimes p_i]$ and $[4^+_1 \otimes p_i]$)$3/2^+$ states (1975, 2017, 2101, 2188 keV) in the energy region of the 0^+_2 and 4^+_1 states of the core nuclei are observed, the first candidate of the three expected $1/2^+$ states is observed at the comparably high excitation energy of 2267 keV. In general, the number of states with spin and parity $1/2^+$ identified is too low compared to the expectations from the particle-core coupling picture.

With regard to the results from the NRF experiment [25], it can be stated that even when some proposed ground-state transitions have been shown in this experiment to be transitions to lower lying excited states arising from states considered to be of $[[2^+ \otimes 3^-] \otimes d_{5/2}]$ nature, the confirmed lack of $E1$ strength compared to both core nuclei provides clear evidence for the suggested Pauli blocking, because the respective transitions are all relatively weak, i.e., they do not provide a considerable amount of $E1$ strength. The smaller deficit of $E2$ strength (80–90%) compared to the the paucity of $E1$ strength (≈60%) can be explained by the multiplicative nature of the $E1$ operator [26,27]$B(E1) \uparrow \propto \beta_2^2\beta_3^2$, where β_2 and β_3 denote the quadrupole and octupole deformations, respectively. Accordingly, a deficit of $E3$ transition strength for the $[3^- \otimes p_j]$ coupled multiplets is to be expected.

B. Negative-parity states

In the odd-mass nucleus ^{141}Pr, there are a number of different ways to create low-lying collective negative-parity states, e.g., the coupling of the intruder orbital to the 2^+_1 quadrupole excitations $[2^+ \otimes h_{11/2}]$, the couplings of the particles in the subshells of the oscillator shell to the 3^- octupole phonon $[3^- \otimes p_j]$ ($p_j = d_{5/2}, g_{7/2}$), and the coupling of the particles to the states of the quadrupole-octupole excitations $[[2^+ \otimes 3^-]_J \otimes p_j](p_j = d_{5/2}, g_{7/2})$. The $[2^+ \otimes h_{11/2}]$ states are expected to decay by $E2$ transitions to the $h_{11/2}$ single-particle state, but the expected signature of $E3$ transitions to the ground state for the octupole-particle coupled states will be obscured by dominating $E1$ transitions. Therefore, unlike the $E2$ decays of the $[2^+ \otimes p_j]$ states, no $E3$ sum rule for the ground-state decays is expected.

For spherical even-even nuclei, the $3^-_1 \rightarrow 2^+_1$ transitions are of $E1$ character and known to set the scale for low-lying $E1$ strength [27] in these nuclei. Both core nuclei have a similar transition strength of $B(E1, 3^-_1 \rightarrow 2^+_1) = (3.8 \pm 0.8) \times 10^{-3}$ W.u. (^{140}Ce), $(4.0 \pm 4.0) \times 10^{-3}$ W.u. (^{142}Nd) [18], but the excitation energies differ by several hundred keV, thus the mixing between the $[3^- \otimes p_j](p_j = d_{5/2}, g_{7/2})$ multiplets should be less than observed for the two discussed $[2^+ \otimes p_j]$ multiplets. Unfortunately, the fact that the dominating transition for these states is the $[3^- \otimes p_j] \rightarrow [2^+ \otimes p_j]$ decay with a comparably small transition energy causes various experimental problems. First, the intensity and, therefore, the experimental uncertainty scale as the $2L + 1$ power of the transition energy. Second, the background in the low-energy part of the spectrum is higher. Third, the transition density in the low-energy region is higher, leading to a higher number of multiplets. Furthermore, for the DSAM method, the momentum transfer between the recoiling nucleus and the emitted γ ray scales with the γ-ray energy, thus the energy shifts are smaller. These factors, along with the tentatively assigned parities and the overall uncertainty of the level scheme for states above 2 MeV, e.g., missing or wrongly placed transitions, make a quantitative comparison difficult. In addition to these experimental difficulties, one has to consider that the final states of these decays are already $\beta_1|2^+ \otimes d_{5/2}\rangle + \beta_2|2^+ \otimes g_{7/2}\rangle$ mixtures. Owing to the $E1$ nature of the decays linking the underlying particle-core coupled components of the respective wave functions, it is not possible to distinguish between the $|3^- \otimes d_{5/2}\rangle \rightarrow |2^+ \otimes d_{5/2}\rangle$ and $|3^- \otimes g_{7/2}\rangle \rightarrow |2^+ \otimes g_{7/2}\rangle$ parts of the transitions based on the observed data. Even the estimate that $\langle 3^- \otimes p_i|\hat{E1}|2^+ \otimes p_j\rangle \propto \sqrt{B(E1)}\delta_{ij}$ is rather crude, because $E1$ transitions are known to be very sensitive to small details of the underlying microscopic structure of the involved states [39,40], thus decays from

TABLE VIII. Candidates for members of the $2^+ \otimes h_{11/2}$ multiplet.

E	J^π	I_γ (%)
1999.8	$13/2^-$	100
2105.0	$15/2^-$	100
2336.3	$(15/2)^-$	55.5
2382.0	$9/2^-$	27.6
2668.8	$13/2^-$	64.5
2707.4	$15/2^-$	100
(2718.4)	(9/2,11/2)	32.0
(2887.5)	(9/2,11/2)	16.9

multiplets coupled with particles in different subshells are also possible. Good examples of these in the pure boson approximation of the core excitation forbidden $E1$ decays are the $|2^+ \otimes p_j\rangle_{9/2} \rightarrow |h_{11/2}\rangle$ transitions (see Fig. 7).

General tendencies of the decay behavior of the states with purported negative parity are that the states around and below 2 MeV near the 3_1^- octupole phonon of ^{142}Nd ($E_{3^-} = 2084$ keV) decay predominantly to the states with a dominant $2^+ \otimes g_{7/2}$ component in their wave functions. The negative-parity states located closer to the octupole phonon of ^{140}Ce ($E_{3^-} = 2464$ keV) preferentially decay to states with a more dominant $2^+ \otimes g_{5/2}$ component. Considering all the uncertainties mentioned above, it is not surprising that for the states with suspected negative parity up to 2.7 MeV, a total strength of $B(E1, [3^- \otimes p_j] \rightarrow [2^+ \otimes p_j]) = 10.7(16) \times 10^{-3}$ W.u. is observed. The decays to the $[2^+ \otimes d_{5/2}]$ states, with half of the decay strength going to the strongly mixed 1292 keV level, yield a summed strength of $B(E1, [3^- \otimes p_j] \rightarrow [2^+ \otimes d_{5/2}]) = 6.7(13) \times 10^{-3}$ W.u. This is nearly twice as much as expected following the decays in the core nuclei, indicating either that some of the parities are wrongly assigned or that some of the decays are incorrectly placed in the level scheme. For the decays to $[2^+ \otimes g_{7/2}]$ dominated states, again 50% of the strength to the 1292 keV level, the total strength results in $B(E1, [3^- \otimes p_j] \rightarrow [2^+ \otimes g_{7/2}) = 4.0(7) \times 10^{-3}$ W.u. This corresponds to the strength observed for the respective transitions in the adjacent core nuclei, but the overall uncertainties cannot be overemphasized.

Candidates for members of the $[2^+ \otimes h_{11/2}]$ multiplet are listed in Table VIII. For some of these states, e.g., the 1999.8 and 2105.0 keV levels, a very large $B(E2)\downarrow$ strength of approximately 60 W.u. is observed, which is unrealistic. Besides the general uncertainties, there may be other explanations, such as strong $M1$ contributions in these transitions or missing stronger transitions; thus the relative γ-ray intensities would be reduced, and, therefore, the $B(E2)$ values decreased.

V. CONCLUSION

In this work, the previously suggested lack of collective transition strength in the odd-mass $N = 82$ isotones due to Pauli blocking was confirmed. Using $(n, n'\gamma)$ techniques, spectroscopic data for states up to 3.15 MeV were obtained. The $[2^+ \otimes p_i](p_i = d_{5/2}, g_{7/2})$ multiplets were identified and interpreted using a two-state mixing approach. Mysteries remaining for these multiplets are the interplay of the $[2^+ \otimes p_i]_{3/2}$ particle-core coupled states with the $d_{3/2}$ subshell and the question of the different mixing strengths, $V_{\rm mix}$, of the different pairs of states with common angular momentum. For further investigation of the interplay of the particle-core coupled $J = 3/2$ states with the $d_{3/2}$ subshell, measurements of the respective multipole-mixing ratios are required. Detailed knowledge of this interplay might give insight into the mechanisms responsible for the fragmentation of single-particle strength.

Nevertheless, deep insight into the nature of the positive-parity states up to nearly 2 MeV has been gained. Above this, the increased level density and enhanced configuration mixing prevent further detailed examination of the state wave functions. Candidates for the $[2^+ \otimes h_{11/2}]$ and for the $[3^- \otimes p_i](p_i = d_{5/2}, g_{7/2})$ negative-parity multiplets were also proposed. The observed behavior of the $[2^+ \otimes p_i](p_i = d_{5/2}, g_{7/2})$ multiplets once more emphasizes the importance of the Pauli exclusion principle in the nucleus, a many-body quantum system. Using the unpaired particle in a subsequent subshell as a probe, we are able to measure the amplitudes of microscopic configurations containing the unpaired particle of the respective core excitation. This fact makes ^{141}Pr an ideal test case for nuclear models, not only to be able to test the application of the Pauli principle, but also to study the underlying microscopic structure of the core excitations.

ACKNOWLEDGMENTS

The authors thank U. Kneissl, N. Tsoneva, V. Werner, N. Pietralla, R. V. Jolos, J. Albrecht, and T. Koch for valuable discussions and information. The careful reading of the manuscript and corrections by D. Judson and A. Petts is appreciated. Furthermore, we are indebted to H. E. Barber for providing excellent proton beams during the experiments. This material is based upon work supported by the U.S. National Science Foundation under Grant Nos. PHY-0354656 and PHY-0652415.

[1] F. Iachello, Phys. Rev. Lett. **53**, 1427 (1984).
[2] U. Kneissl, N. Pietralla, and A. Zilges, J. Phys. G **32**, R217 (2006).
[3] N. Pietralla, P. von Brentano, and A. F. Lisetskiy, Prog. Part. Nucl. Phys. **60**, 225 (2008).
[4] P. E. Garrett, K. L. Green, H. Lehmann, J. Jolie, C. A. McGrath, M. Yeh, and S. W. Yates, Phys. Rev. C **75**, 054310 (2007).
[5] A. Bohr and B. R. Mottelson, K. Dan. Vidensk. Selsk. Mat. Fys. Medd. **27**, no. 16, 1 (1953).
[6] A. Bohr and B. R. Mottelson, *Nuclear Structure*, Vol. 2 (Benjamin, New York, 1975).
[7] N. Sandulescu and R. J. Liotta, J. Phys. G **20**, 2001 (1994).
[8] R.-D. Herzberg, Ph.D. thesis, Universität zu Köln, 1995.

[9] V. G. Soloviev, *Theory of Complex Nuclei* (Pergamon, Oxford, 1976).
[10] V. G. Soloviev, *Theory of Atomic Nuclei, Quasiparticles and Phonons* (IOP, London, 1992).
[11] P. von Neumann-Cosel, V. Yu. Ponomarev, A. Richter, and C. Spieler, Z. Phys. A **350**, 303 (1995).
[12] V. Yu. Ponomarev, J. Bryssinck, L. Govor, F. Bauwens, O. Beck, D. Belic, P. von Brentano, D. De Frenne, C. Fransen, R.-D. Herzberg, E. Jacobs, U. Kneissl, H. Maser, A. Nord, N. Pietralla, H. H. Pitz, and V. Werner, Phys. Rev. Lett. **83**, 4029 (1999).
[13] J. Bryssinck, L. Govor, V. Yu. Ponomarev, F. Bauwens, O. Beck, D. Belic, P. von Brentano, D. De Frenne, T. Eckert, C. Fransen, K. Govaert, R.-D. Herzberg, E. Jacobs, U. Kneissl, H. Maser, A. Nord, N. Pietralla, H. H. Pitz, and V. Werner, Phys. Rev. C **61**, 024309 (2000).
[14] K. Heyde, P. Van Isacker, M. Waroquier, J. L. Wood, and R. A. Meyer, Phys. Rep. **102**, 291 (1983).
[15] A. Adam, O. Bersillon, and S. Joly, in *Proceedings of the Third All-Union Conference on Neutron Physics, Kiev, 1975* (TsNIIatominform, Moscow, 1976), Vol. 5, p. 48.
[16] B. H. Wildenthal, E. Newman, and R. L. Auble, Phys. Rev. C **3**, 1199 (1971).
[17] P. D. Clark, T. R. Ophel, J. S. Eck, A. F. Zeller, J. Nurzynski, D. C. Weisser, and D. F. Hebbard, Nucl. Phys. **A349**, 258 (1980).
[18] www.nndc.bnl.gov/ensdf/.
[19] M. Grinberg, T. K. Dinh, C. Protochristov, I. Penev, C. Stoyanov, and W. Andrejtscheff, J. Phys. G **19**, 1179 (1993).
[20] M. Grinberg and Ch. Stoyanov, Nucl. Phys. **A573**, 231 (1994).
[21] K. Heyde, *The Nuclear Shell Model*, 2nd Ed. (Springer-Verlag, New York, 1994).
[22] R.-D. Herzberg, I. Bauske, P. von Brentano, Th. Eckert, R. Fischer, W. Geiger, U. Kneissl, J. Margraf, H. Maser, N. Pietralla, H. H. Pitz, and A. Zilges, Nucl. Phys. **A592**, 211 (1995).
[23] R. D. Heil, B. Kasten, W. Scharfe, P. A. Butler, H. Friedrichs, S. D. Hoblit, U. Kneissl, S. Lindenstruth, M. Ludwig, G. Müller, H. H. Pitz, K. W. Rose, M. Schumacher, U. Seemann, J. Simpson, P. von Brentano, Th. Weber, C. Wesselborg, and A. Zilges, Nucl. Phys. **A506**, 223 (1990).
[24] H. H. Pitz, R. D. Heil, U. Kneissl, S. Lindenstruth, U. Seemann, R. Stock, C. Wesselborg, A. Zilges, P. von Brentano, S. D. Hoblit, and A. M. Nathan, Nucl. Phys. **A509**, 587 (1990).
[25] M. Scheck, P. von Brentano, C. Fransen, U. Kneissl, C. Kohstall, A. Linnemann, D. Mücher, N. Pietralla, H. H. Pitz, C. Scholl, F. Stedile, S. Walter, V. Werner, and S. W. Yates, Phys. Rev. C **75**, 044313 (2007).
[26] A. Bohr and B. R. Mottelson, Nucl. Phys. **4**, 529 (1957).
[27] N. Pietralla, Phys. Rev. C **59**, 2941 (1999).
[28] P. E. Garrett, N. Warr, and S. W. Yates, J. Res. Natl. Inst. Stand. Technol. **105**, 141 (2000).
[29] E. Sheldon and V. C. Rogers, Comput. Phys. Commun. **6**, 99 (1973).
[30] E. Storm and H. I. Israel, Nucl. Data Tables **7**, 565 (1970).
[31] http://www.nndc.bnl.gov/exfor7/endf00.htm.
[32] E. Sheldon and D. M. van Patter, Rev. Mod. Phys. **38**, 143 (1966).
[33] K. B. Winterbon, Nucl. Phys. **A246**, 293 (1975).
[34] U. Kneissl, H. H. Pitz, and A. Zilges, Prog. Part. Nucl. Phys. **37**, 349 (1996).
[35] H. J. Rose and D. M. Brink, Rev. Mod. Phys. **39**, 306 (1967).
[36] J. K. Tuli and D. F. Winchell, Nucl. Data Sheets **92**, 332 (2001).
[37] K. Andhradev, V. N. Kulkarni, and R. G. Kulkarni, J. Phys. Soc. Jpn. **49**, 448 (1980).
[38] T. Ahn, N. Pietralla, G. Rainovski, A. Costin, K. Dusling, T. C. Li, A. Linnemann, and S. Pontillo, Phys. Rev. C **75**, 014313 (2007).
[39] V. Yu. Ponomarev, Ch. Stoyanov, N. Tsoneva, and M. Grinberg, Nucl. Phys. **A635**, 470 (1998).
[40] R. V. Jolos, N. Yu. Shirikova, and V. V. Voronov, Phys. Rev. C **70**, 054303 (2004).